Engineering Structures 310 (2024) 118130

Contents lists available at ScienceDirect

Engineering Structures

journal homepage: www.elsevier.com/locate/engstruct

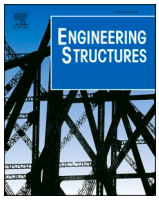

Computational prediction of impact sound insulation of a full-scale timber floor applying a FEM simulation procedure

Jesse Lietzén [a,*], Ville Kovalainen [b], Mikko Kylliäinen [a], Sami Pajunen [a]

[a] Faculty of Built Environment, Unit of Civil Engineering, Tampere University, Finland
[b] AINS Group, Department of Acoustical Engineering, Finland

ARTICLE INFO

Keywords:
Impact sound insulation
FEM
Tapping machine
Timber floor

ABSTRACT

During the recent decades, simulation procedures involving the finite element method (FEM) have been developed to enable prediction of impact sound insulation of timber slabs and floors. FEM simulations have previously been applied for timber floors mainly in low frequencies despite their evident ability to operate over a wide frequency range. Additionally, the validation processes have involved calibrations and experimental modal analyses which can seldom be performed in product development tasks concerning full structures. The purpose of this research was to study the applicability of a FEM simulation procedure to predict normalised impact sound pressure levels L_n of a full-scale timber floor if material data provided by the product manufacturers is used. The floor was studied at three construction stages where the FEM simulations were performed for the bare floor and the rib slab, and the floor covering was considered in the post-processing stage in case of the full floor. The impact force excitation generated by the ISO standard tapping machine was described with the recently published procedure involving explicit dynamics analysis. To serve the purposes of this study, the FEM models were fully constructed before the measurements were carried out. According to the results, the 1/3-octave L_n of the full floor and the floor without covering was predicted with a 0 to 9 dB accuracy depending on the frequency band and the single-number quantities with a 0 to 4 dB accuracy. The single-number quantities of the bare rib slab were underestimated with the simulations by 4 to 5 dB. Probable causes for the discrepancies between the simulation and measurement results pointed mainly to the uncertain material properties but possibilities for modelling inaccuracies could not be excluded.

1. Introduction

Impact sound insulation (ISI) is one of the principal technical parameters dimensioning the structural layers of timber floors in apartment buildings. For this reason, evaluating the ISI of the floor is probably the most important task of acousticians working in timber construction projects. Instead of choosing the acoustical solutions for the floor based on experience gained in previous projects or from field or laboratory measurements, an appealing approach would be to use prediction tools to evaluate the ISI of the floor. The ability to assess the ISI using computational methods would ease the work of acoustical engineers in the design phase of the building. Moreover, it would enable the development of novel timber floors or associated products aimed for timber construction markets. However, one problem is that standardised methods [1] for calculating the ISI are not applicable to lightweight timber floors. For this reason, several strategies for calculating the ISI of timber floors from analytical to numerical models have been shown in the research literature [2,3]. This paper is focusing on the ISI prediction of timber floors with numerical methods (later briefly called *simulations*) with an emphasis on simulating the normalised impact sound pressure levels L_n generated by the ISO standard tapping machine (STM) [4,5], which is probably the most widely used standardised impact sound source in Europe, as far as regulations are concerned [6]. Due to the chosen simulation methodologies, the procedures applied here are currently mainly fit for research and product development purposes of timber floors.

Since the beginning of the 21st century, simulating the low-frequency (below 500 Hz, usually below 250 Hz) ISI of floors has been a topical research subject. The main simulation method has been the finite element method (FEM), but also the finite-difference time-domain (FDTD) method and hybrid methods together with the statistical energy analysis (SEA) have been applied. The following paragraphs aim to

* Corresponding author.
E-mail address: jesse.lietzen@tuni.fi (J. Lietzén).

https://doi.org/10.1016/j.engstruct.2024.118130
Received 3 August 2023; Received in revised form 7 April 2024; Accepted 26 April 2024
Available online 6 May 2024

review the research literature concerning the simulations performed to investigate acoustical behaviour related to ISI performance of different types of floors and slabs with a focus on timber structures.

For concrete slabs and floors, all the abovementioned simulation methods have successfully been used. FDTD has been applied by Asakura [7,8] to simulate the radiated impact sound generated by a bang machine and a standard rubber ball on concrete floors equipped with light weighted floor surface structures and suspended ceilings. Hybrid FEM-SEA methods have been used by Cho [9,10] and Kim et al. [11,12] to analyse the behaviour of floating floors on a concrete slab, and to simulate the radiated impact sound of a concrete mock-up structure excited with an impact hammer and a bang machine, respectively. Park and Kim [13] used FEM to model the impact sound in a concrete mock-up structure excited with a bang machine and a standard rubber ball. Furthermore, Jean et al. [14] and Vastiau et al. [15]. have used FEM to simulate the impact sound pressure level generated by the STM on concrete slabs. Their studies differ from the aforementioned studies [7–13] so that their computations covered a broad frequency range up to 1000 Hz [14] and 5000 Hz [15] in addition to the low frequencies.

FEM has widely been used to assess the low-frequency vibration (related to the acoustical performance) of timber slabs and floors. Bard et al. [16], Negreira et al. [17] and Shen and Hopkins [18–20] have examined the low-frequency vibrational performance of timber rib slabs excited with a single hammer of STM, an impact hammer, and a standard rubber ball, respectively. Negreira and Bard [21] also simulated vibration of a timber rib slab excited with a single hammer of STM. Persson and Flodén [22] have investigated the effect of the material property variation on the vibration response of a timber rib slab. Mass timber slabs have been studied by Filippoupolitis et al. [23,24] who simulated the vibration of a mass timber slab formed from dowel-connected joists, and by Qian et al. [25,26] who studied the vibration generated by an impact hammer and a STM on a cross-laminated timber (CLT) slab. In the project Silent Timber Build, Bard et al. [27] modelled the low-frequency vibrational velocity levels of different timber floors excited with the STM. Moreover, FEM has been used to simulate the vibration performance of full-scale timber mock-up structures by Bolmsvik et al. [28,29] and Flodén et al. [30]. Thus, FEM has proven to be a versatile tool to evaluate different vibrational phenomena occurring in timber structures.

The vibration performance and the sound radiation of structures are closely related and thus, FEM has been applied to simulate the low-frequency sound radiation of point-excited timber slabs and floors. For example, Hopkins et al. [31] have simulated the radiation efficiency of the mass timber slab formed from dowel-connected joists by applying an acoustic-structure interaction (ASI) model where the sound radiation into an infinite room was computed with the FEM model. Buchschmid et al. [32] and Kohrmann et al. [33] computed the radiated sound power level of a CLT slab based on its vibrational velocity via an integral transform post-processing method. The sound radiation of hollow-core concrete and hybrid timber slabs have been computed by Olsson et al. [34] by applying an analytical model of an infinite air duct to solve the radiation from a point load excited FEM model, and by Linderholt and Olsson [35] by simulating the sound radiation of the slabs excited by human footsteps into an infinite air duct using FEM. Additionally, Olsson and Linderholt [36] have modelled the radiated sound pressure level of point-excited timber rib slab floors by applying the method from ref. [35]. These studies show that there are several possibilities to solve the sound radiation from vibrating timber structures.

In addition to the concrete floors and slabs [13–15], FEM has previously been applied to simulate the low-frequency ISI of timber floors. Rabold [37] and Rabold et al. [38–40] computed the impact sound pressure levels of timber floors in the low-frequency range below 250 Hz. To describe the impact force excitation generated by the STM they applied a general impact force model [41] in their computations where the vibrational behaviour of the floors was solved with a modal superposition method. Thus, the air cavities of the floors were not considered, and porous materials of the timber floors were modelled as a linear elastic solid media [37]. However, there is evidence that air and porous materials should be modelled as acoustic fluid and porous material models, respectively, due to their effect on the vibrational behaviour of timber structures even in the low-frequency range [30,32]. Instead of a modal superposition method, Kohrmann [42] and Kohrmann et al. [43] simulated the radiated sound power level of timber floors in the low-frequency range below 200 Hz by applying a full harmonic analysis together with ASI to couple the acoustical and structural domains of the timber floors equipped with air cavities. To consider the impact force excitation generated by the STM, however, they multiplied the computed transfer functions with the load spectra determined with a simple impact force model [44] mainly suitable for describing the interaction between the STM and concrete floors [42,43]. Additionally, Coguenanff [45] has modelled the radiated impact sound pressure level of a timber rib slab floor excited with a STM in the low-frequency range below 250 Hz. He used a probabilistic model [45,46] to describe the behaviour of the STM on the floor.

Although FEM is regarded as a tool for low-frequency computations, partly due to the computational resources needed, there is evidence that FEM can be used in ISI simulations in a broad frequency range [14,15]. Furthermore, Wang et al. [47] recently presented a FEM model successfully simulating the radiated impact sound pressure level of a timber rib slab excited with a STM in frequencies up to 4000 Hz. They described the excitation of the slab by applying the general impact force model presented by Brunskog and Hammer [48]. The satisfactory agreement between the simulated and measured impact sound pressure levels [47] implies that accurate mid- and high frequency ISI simulations of timber floors are possible by applying FEM if the material properties and the modelling procedures are well known.

According to the authors' knowledge, models predicting the radiated impact sound pressure level generated by the STM on full timber floors that apply validated FEM models in a broad frequency range have not been published so far. The term full floor, in this respective, means that the floor under investigation has all the structural and acoustical layers (a load-bearing timber slab, a structural surface layer to add mass of the slab, a suspended ceiling, and absorptive material in the air cavity), and that the dimensions of the floor also correspond to the dimensions of a room in an apartment building. The presented research literature shows no examples of FEM simulations corresponding with ISI laboratory measurements of timber floors other than at low frequencies. At larger frequencies, also the effect of the floor covering on the ISI must be considered. This can simply be performed within post-processing provided that the measurement result for the improvement of impact sound insulation (ΔL) is available. Moreover, another important point of view is that the material parameters used in the FEM models for timber slabs and floors presented in the literature have either been selected from the literature (e.g., [27,37,42,45]) or determined through experimental modal analysis (e.g., [23,24,32,47]) which are also applied to test the validity of the modelling procedure. Especially for product development purposes, the aim for simulation tools is to predict the ISI of floors by using information from material properties provided by manufacturers, i.e., mechanical properties, density, and possibly loss factors. Moreover, for this purpose, experimental modal analyses can seldom be carried out to determine the input data or modelling procedure. To assess the possibility to use FEM in the product development, the models should be applied with the given information from the properties of the studied materials supplemented with information from the literature if needed. Additionally, the best possible information for the modelling procedure should be used.

The purpose of this study is to assess applicability of a state-of-the-art FEM procedure to imitate the ISI laboratory measurements of a full-scale timber floor. The proposed FEM models predicting the normalised impact sound pressure level L_n of the STM driven floor without the floor covering and the bearing timber slab were created with material data presented by the product manufacturers and validated against the

laboratory measurements. The impact force excitation generated by the STM was described with the recently published procedure involving explicit dynamics analysis [49]. To demonstrate the ISI prediction process of the full floor with the floor covering, the simulation results of the floor without the floor covering were supplemented with ΔL measurement results. Rather than focusing solely on the low-frequency impact sound insulation, the computations were also performed for higher frequencies up to 1000 Hz 1/3-octave band. This frequency range was chosen since it usually dimensions the single-number quantities (SNQs) of ISI of timber apartment floors [50], although in general frequencies up to 3150 Hz are considered in the measurements. One practical application of the applied procedure is to assess the ISI of a timber floor in a broad frequency range during its product development phase prior to laboratory measurements.

2. Materials and methods

2.1. Floor structure

The structure under study was a full timber floor with a rib slab as its bearing structure. In addition to the rib slab, the full floor F1 consisted of a floor covering, plasterboards attached onto the slab, a suspended plasterboard ceiling, and a glass wool layer installed between the ribs (Fig. 1). The floor was studied in three stages F1 (the full floor), F2 (the floor without floor covering), and F3 (the bare rib slab), as depicted in Fig. 1. The ISI of the floor in its construction stages F2 and F3 was first simulated and then the floor was measured in a laboratory in all its stages F1, F2, and F3.

The whole cross section in transversal direction for the floor F1 has been shown in Fig. 2. The width of the floor was 3020 mm, and the length 3870 mm. The rib slab was constructed from 27 mm thick laminated veneer lumber (LVL) panel deck and 45 × 260 mm LVL beams (c/c 490 mm). Between the two side beams, 45 × 100 mm secondary LVL beams (c/c 550 mm) were installed on both sides of the rib slab to support the end of the ceiling structures. These secondary beams were attached to the main beams of the rib slab. In the fabrication of the bare rib slab F3, all the LVL products were both screwed and glued to each other. The two plasterboard layers of thickness 15.5 mm had paper liners (carton) with an approximate thickness 0.5 mm on both sides of the boards. The boards were glued on the top of the LVL panel deck and to each other. Additionally, the plasterboards were screwed from their corners to the underlying layers. The ceiling included two plasterboard layers of thickness 12.5 mm suspended from the rib slab with LVL battens. These plasterboards were installed with screws (c/c 200 mm along the battens). The overhead boards of the LVL battens were of the same material than used for the LVL panel deck of the rib slab. The lower battens were sawn from similar LVL beams than used in the rib slab. The battens were screwed to each other and to the main and secondary beams with a single screw at each junction. The air cavity within the structure was absorbed by installing a 95 mm layer of glass wool between the ribs. The floor covering installed onto the floor F1 was a 14 mm thick multilayer parquet (oak) equipped with tongue-and-groove joints. The parquet was installed on a soft underlayment of thickness 3 mm.

The floors were supported to the laboratory opening at their short ends by elastomer strips (Sylomer® SR 42, thickness of 12.5 mm) installed between the LVL beams of the rib slab and the supporting steel frame of the opening (Fig. 3, detail 1). The end steel frame attached to the rest of the structures in the laboratory opening had a thickness of 10 mm and five steel ribs below the frame with an equal spacing (c/c 600 mm). The long edges and other structural components were kept mechanically unattached to the supporting frame apart from the compounds and linen wool installed between the floors and the frame for sealing purposes (Fig. 3). Thus, the floors were elastically supported only in the direction of the bearing LVL beams with a span of 3850 mm. Additionally, due to the supporting structures of the laboratory opening, the radiative surface below the floor, i.e., the suspended plasterboard ceiling, was smaller than the area of the rib slab itself. The longitudinal dimension of the ceiling was 3680 mm, and transversal 2830 mm. To prevent sound radiation from the sides of the frame, sawn timber studs and plasterboards were installed under the frame. This installation added total mass below the frame by 37.8 kg/m^2.

2.2. Simulations

Computations were performed to predict the ISI laboratory measurements of the floor structure in its construction stages F1, F2 and F3. The predictions were carried out according to the procedure presented below (Section 2.2.1) applying FEM simulations and post-processing methods to compute the normalised impact sound pressure levels L_n of the floors in the frequency range enveloping the 1/3-octave bands 50–1000 Hz.

2.2.1. FEM procedure for determining the impact sound pressure level of a timber floor excited by the STM

Impact sound pressure level generated by a STM on the timber floors F1, F2 and F3 was computed in a frequency domain by applying a three-stage method illustrated in Fig. 4. The actual FEM simulations were carried out for the floor F2 (the floor without floor covering) and F3 (the bare rib slab). The prediction result of L_n for the full floor F1 was achieved simply with a difference between the results for the floor F2 and for the measured improvement of impact sound insulation (ΔL) of the floor covering. This was performed to demonstrate the application of the proposed FEM procedure for the full timber floor.

At the first stage, impact force excitation generated by an ISO tapping machine was determined. Instead of using available impact force models (e.g., [41,46,48,51,52]) to describe the excitation, the force pulses generated by single hammers impacting on the floors F2 and F3

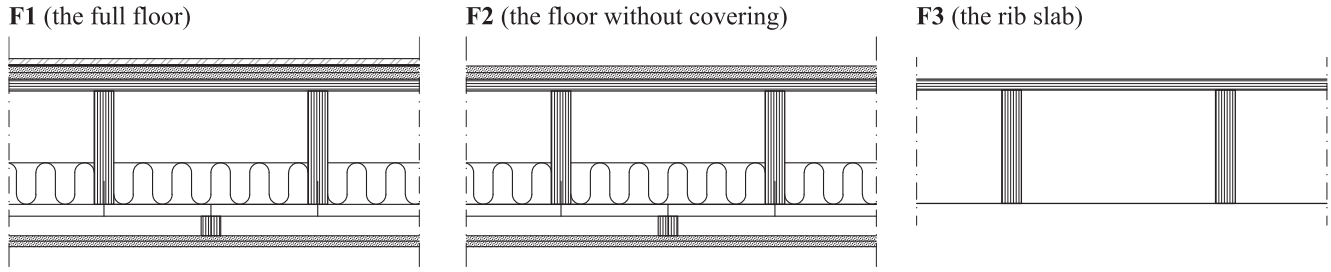

Fig. 1. Floor structure F1 and its construction stages F2 and F3. The layers of the floor F1 from top to bottom were as follows: a multilayer parquet (thickness h = 14 mm) on an underlayment (h = 3 mm), two plasterboard layers (h = 15.5 mm), rib slab with a LVL deck (h = 27 mm) and LVL beams (h = 260 mm, width b = 45 mm, c/c = 490 mm), a glass wool layer (h = 95 mm) between the ribs, overhead boards from LVL deck (h = 27 mm, b = 100 mm, c/c = 550 mm) screwed below the ribs, LVL battens from LVL beams (h = 45 mm, b = 45 mm, c/c = 490 mm) screwed to the overhead boards between the ribs, and two plasterboard layers (h = 12.5 mm). The floor F2 corresponded with the floor F1 apart from the floor covering. The floor F3 consisted only of the rib slab.

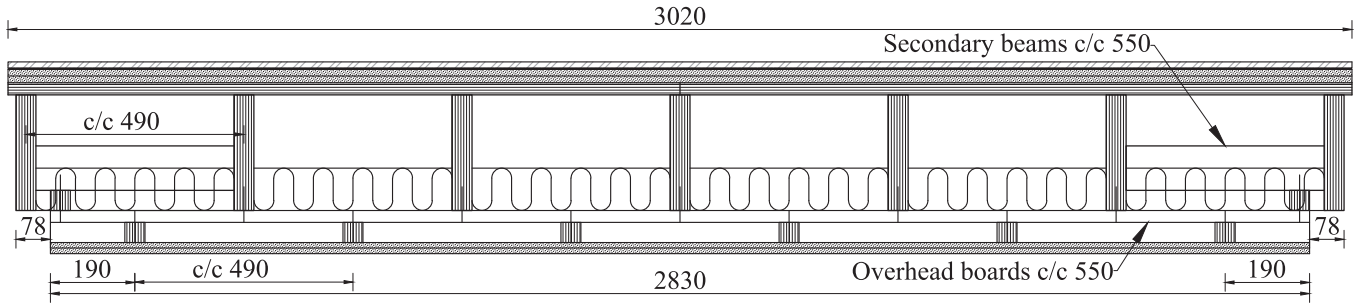

Fig. 2. Schematic cross section of the floor F1 in transversal direction, dimension in millimetres. The width of the floor was 3020 mm, and the length 3870 mm. The width of the ceiling was 2830 mm, and the length 3680 mm.

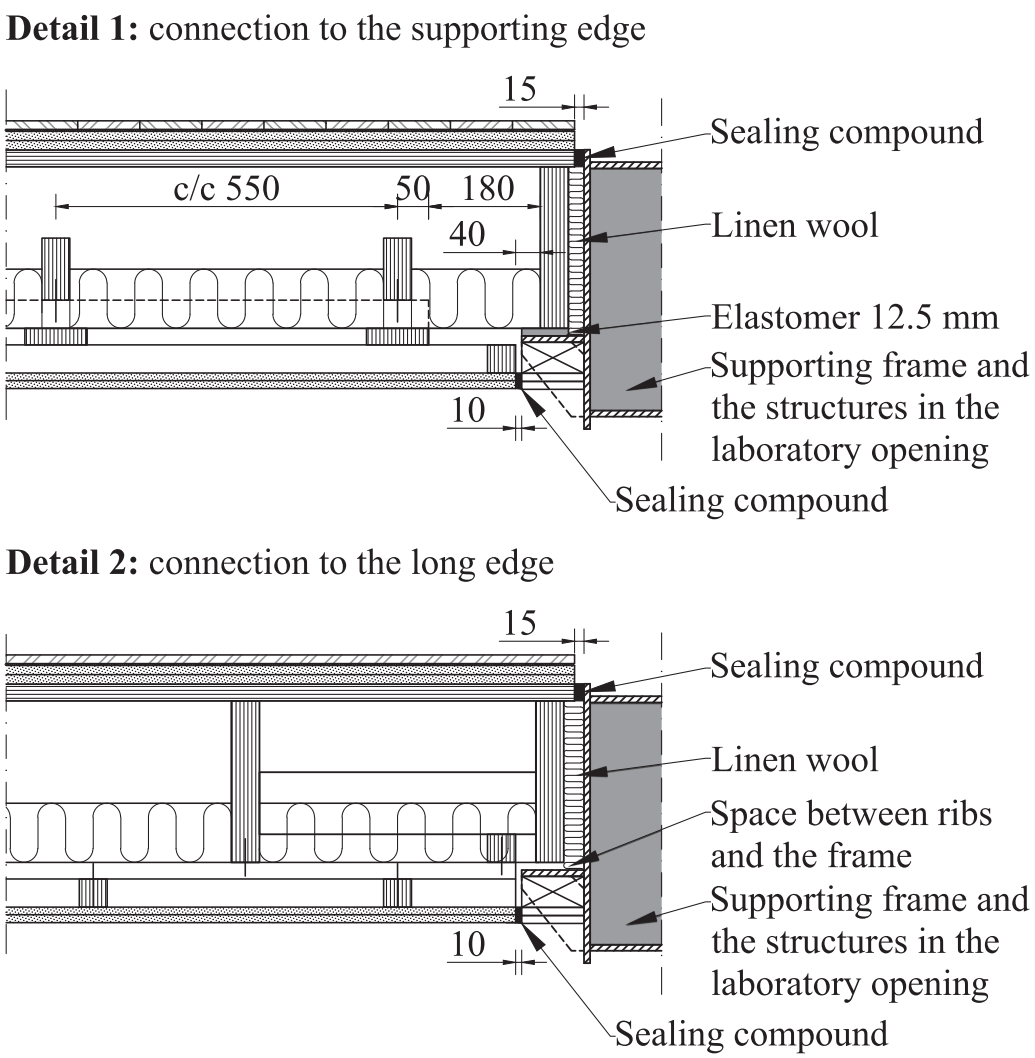

Fig. 3. Floor supporting details. Dimensions in millimetres.

were simulated by using explicit dynamics analysis with Ansys LS-DYNA (smp s R10.1.0 Revision: 123,264) following the procedures presented in the ref. [49]. This way, the time histories of the impact forces were computed with a FEM model considering the non-linear behaviour of the contact between the hammers and the floor. With a post-processing method [48,49,52], the impact force pulses were converted into frequency domain to present continuous operation of the STM. As a result, complex 2 Hz line spectra presenting the five individual point forces driving the floors were derived.

The second stage involved FEM simulations of the impact sound radiation of the floors F2 and F3 excited by the previously determined point forces describing the behaviour of the STM hammers on the floors. At this stage, the computations were performed in frequency domain to provide accurate results with less computational effort than with simulations in the time domain [21]. Thus, the system was modelled as linear. Since in general, the timber floors can consist of structural parts, air cavities and porous materials, a fully coupled harmonic multiphysics analysis was applied. The simulations were performed by using COMSOL Multiphysics 6.1 with a 2 Hz frequency resolution which corresponds to the excitation line spectra of a STM. In the analysis, the

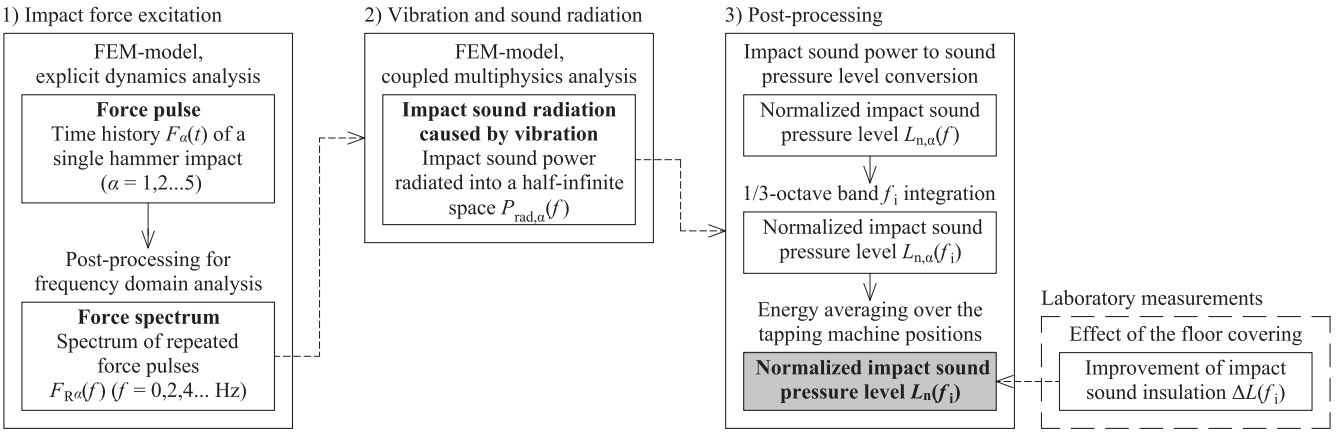

Fig. 4. A three-stage FEM procedure to determine the normalised impact sound pressure level L_n of a timber floor excited by a STM.

radiated sound powers of the floors F2 and F3 were solved directly with the FEM model by applying an acoustical fluid domain below the floor. Moreover, this domain was set to present an acoustical half-infinite space. The fully absorptive boundary conditions were set to the faces of the domain (excluding the radiating plane) by applying perfectly matched layers (PML) [53]. Thus, the approach slightly differed from the methods shown in the literature [31,35,36]. The governing equations concerning the simulations at this stage have been presented in Section 2.2.2.

At the third stage, the simulated results presenting the radiated sound power were post-processed to present the normalised impact sound pressure levels L_n in a receiving room. First the narrow-band sound power results were converted to present the normalised impact sound pressure level L_n in a diffuse sound field, and second, the results were integrated to present the 1/3-octave band results. The last part involved energy averaging over the STM positions. Since the aim of the procedure is to be applicable to research and product development of timber floors, the effect of the floor covering on the ISI (in case of the full floor F1) was introduced in the post-processing stage where information from the laboratory measurements of the improvement of impact sound insulation (ΔL) was used. This corresponds to an engineering task where the floor covering is chosen based on the performance of the bare floor. Because it has been noted that the floor coverings should be measured on a floor representing the behaviour of the timber floor under study [54], the ΔL of the floor covering under study was calculated from the ISI laboratory measurements (see Section 2.4).

2.2.2. Governing equations

The system describing the frequency-dependent impact sound radiation of the timber floors consisted of three different types of domains: structural Ω_s, acoustical Ω_a and poroacoustical domains Ω_{pa}. In the simulations, these domains were coupled, where two-way interaction was present. The partial differential equation of motion describing the system inside the structural domains Ω_s in the frequency domain was:

$$\nabla\cdot\boldsymbol{S} + \mathbf{F}_V e^{i\phi} = -\rho\omega^2\mathbf{u} \tag{1}$$

where $\boldsymbol{S}$ denotes the second Piola-Kirchoff stress tensor, $\mathbf{F}_V$ is the harmonic volume force vector, ϕ is the corresponding phase, $i = \sqrt{-1}$ represents the imaginary unit, ρ is the material dependent density, $\omega = 2\pi f$ is the angular frequency where f is the frequency, and $\mathbf{u} = \mathbf{u}(\boldsymbol{x},\omega) = \mathbf{u}(\boldsymbol{x})e^{i\omega t}$ is the displacement [55]. The structural domain comprised of all the components of the studied floors apart from the mineral wool and the air cavities within the floors.

Damping in the structural domains was introduced by applying material-dependent loss factors η_s (i.e., structural damping coefficients). Thus, the constitutive elasticity matrix $\boldsymbol{D}$ was converted into complex constitutive matrix $\boldsymbol{D}^c$ as follows:

$$\boldsymbol{D}^c = (1 + i\eta_s)\boldsymbol{D} \tag{2}$$

In the analysis, the structural domain was driven by the five point sources with individually predetermined force spectra representing the continuous operation of the five hammers of the STM in the respective source position (for the method description, see Section 2.2.1, and ref. [49]). The other boundary conditions of the domain were the ASI interfaces and the prescribed displacements representing the floor supports.

In the acoustical Ω_a and poroacoustical domains Ω_{pa} governed the homogeneous Helmholtz equation (without the acoustical domain sources) with a linear elastic fluid model:

$$\nabla\cdot\left(-\frac{1}{\rho_c}\nabla p\right) - \frac{\omega^2 p}{\rho_c {c_c}^2} = 0 \tag{3}$$

where $p = p(\boldsymbol{x},\omega) = p(\boldsymbol{x})e^{i\omega t}$ denotes the time-harmonic sound pressure, and t is the time [53]. For acoustical domains, i.e., the air cavities and the airspace below the floor, the density $\rho_c = \rho_{air}$ was 1.21 kg/m^3, and the speed of sound $c_c = c_{air}$ was 343 m/s. For the poroacoustical domains, i.e., the mineral wools in the cavities, an equivalent fluid model originating from the empirical model of Delany and Bazley [56] was applied. Here the Helmholtz equation was solved with modified complex values for the speed of sound c_c and density ρ_c based on the material data from the mineral wools:

$$c_c = \frac{c}{\left(1 + C_1\left(\rho_f\frac{f}{R_f}\right)^{-C_2} - iC_3\left(\rho_f\frac{f}{R_f}\right)^{-C_4}\right)} \tag{4}$$

$$\rho_c = \frac{\rho_f c}{c_c}\left(1 + C_5\left(\rho_f\frac{f}{R_f}\right)^{-C_6} - iC_7\left(\rho_f\frac{f}{R_f}\right)^{-C_8}\right) \tag{5}$$

where R_f represents the static airflow resistivity, and $\rho_f = \rho_{air}$ is the density of the fluid saturating the fibrous material [53]. Instead of the original values for the empirical coefficients from C_1 to C_8, we applied the modified Allard and Champoux model [53,57], since the model has been noticed to accurately predict the sound absorption of different mineral wool configurations [58].

Two boundary conditions were present for the acoustical and poroacoustical domains. First, the open sides of the acoustical cavity parallel to the edges of the laboratory opening, and the upper part of the receiving acoustical volume had sound hard boundaries where the Eq. (6) holds:

$$-\mathbf{n}\cdot\left(-\frac{1}{\rho_c}\nabla p\right) = 0 \tag{6}$$

where **n** denotes the surface normal [53].

Secondly, coupling the acoustical and poroacoustical domains with the structural domains requires determining ASI interfaces. This boundary condition between the domains was valid both inside the floor between the beams, plates, and the acoustical cavities, and below the floor between the lowest plasterboards and the receiving half-infinite airspace. Mathematically, the ASI between the different sides (up and down) of the interaction within the floor is described with Eqs. (7–9):

$$-\mathbf{n}\cdot\left(-\frac{1}{\rho_c}\nabla p_t\right)_{up} = -\mathbf{n}\cdot\mathbf{u}_{tt} \tag{7}$$

$$-\mathbf{n}\cdot\left(-\frac{1}{\rho_c}\nabla p_t\right)_{down} = -\mathbf{n}\cdot\mathbf{u}_{tt} \tag{8}$$

$$\mathbf{F}_A = \left(p_{t,down} - p_{t,up}\right)\mathbf{n} \tag{9}$$

where p_t is the total acoustic pressure, $\mathbf{F}_A$ is the load per unit area of the structure, and $\mathbf{u}_{tt}$ is the structural acceleration of the specific boundary [53].

At the exterior boundary where the lower plasterboards radiate into the airspace below, the ASI was [53]:

$$-\mathbf{n}\cdot\left(-\frac{1}{\rho_c}\nabla p_t\right) = -\mathbf{n}\cdot\mathbf{u}_{tt} \tag{10}$$

$$\mathbf{F}_A = p_t\mathbf{n} \tag{11}$$

2.2.3. Model settings and geometry

Main geometries of the simulation models have been illustrated in Fig. 5 for the floors F2 and F3 together with their computational meshes at 1000 Hz. In addition to the floor, the FEM models included the airspace below the floor surrounded with the PML. This acoustical boundary condition corresponded to an infinite baffle surrounding the floor specimen. The thickness of the airspace and the PML was a quarter of a wavelength in the acoustic domain for each frequency studied. The floors were supported in both vertical and horizontal directions from the bottom sides of the elastomers (shown in red in Fig. 5).

The models of the floors F2 and F3 were constructed two different ways. In both cases the plasterboards were modelled as continuous solid layers. First, the models were created to represent *ideal* boundary conditions and constraints. This is comparable to a product development task, where idealisation is needed since the exact conditions of the structures are usually not known. On the other hand, the purpose of the idealisation is to gain results of the structure independent of the measurement facilities. In the second stage, the models were modified to consider the in-situ boundary conditions and constraints of the laboratory measurements. This way, the effect of boundary conditions and smaller details can be analysed. The simulated versions were:

- Ideal
  - Ideal boundary conditions (see Fig. 2):
    - Rib slab was supported from the bottom sides of the elastomers
    - Free boundary conditions along the periphery of the rib slab
    - Free boundary conditions along the periphery of the ceiling plasterboards (only F2)
  - Constraints of the ceiling (only F2):
    - Line contacts between the battens and plasterboards representing the screw rows
- In-situ
  - In-situ boundary conditions (see Section 2.4):
    - Rib slab was supported from the bottom sides of the elastomers with the steel frame of the laboratory opening (the parts of the frame below the elastomers were modelled)
    - Sealing compound around the periphery of the LVL deck of the rib slab
    - Sealing compounds around the periphery of the ceiling plasterboards (only F2)
    - Cavities between the laboratory opening and the floor boundaries (only F2)
  - Constraints of the ceiling (only F2):

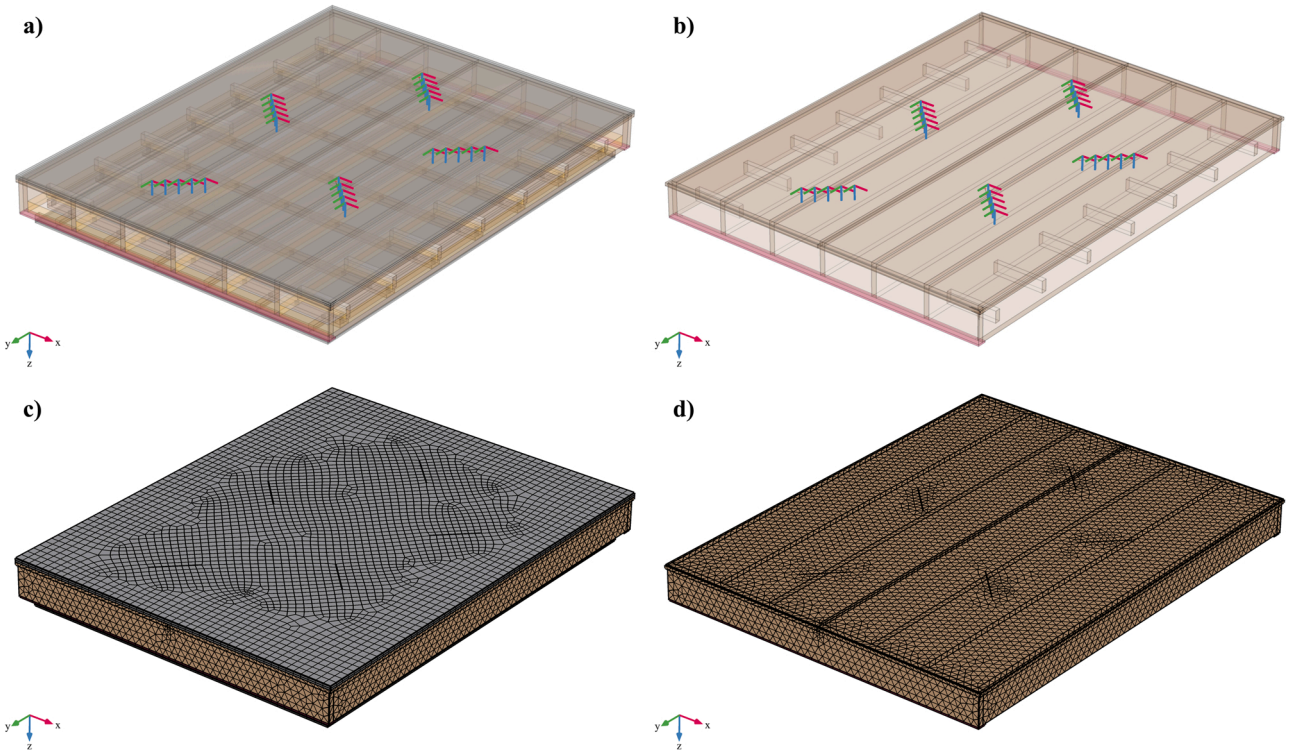

Fig. 5. Geometry and mesh (at 1000 Hz) of the FEM models for the floors F2 (a, c) and F3 (b, d). Note that the airspace and the PML below the floor have been hidden to highlight the structural features of the floor.

- Point contacts between the battens and plasterboards representing the individual screws.

The point contacts induced by the screws between the beams, boards, battens, and plasterboards were described by constraining the three-dimensional displacements of destination and source points to be equal.

The screw rows between the ceiling battens and plasterboards were considered as line constraints in a similar manner in the models representing the ideal cases. The contacting boundaries of the ceiling plasterboards were presented in all cases with no separation constraints allowing the parts sliding in parallel direction with the boundaries but not separating from each other. To study the effect of the ceiling contacts (between the beams and overhead boards, the ceiling battens and overhead boards, the secondary beams and ceiling battens, ceiling battens and plasterboards) on the results, no separation constraints were applied between the counter surfaces of the beams, boards, battens, and plasterboards in addition to the point constraints. These were considered only in the results presented in Section 2.3.

The frequency-dependent element mesh consisted of quadratic hexahedral and tetrahedral Lagrange elements. The minimum criteria for the mesh density to be met was to achieve at least five elements per wavelength in all the domains to represent the waves on the mesh. In case of the structural domains, bending waves were taken into account in the requirements considering that the structures behave as ribbed plates [59]. The number of degrees of freedom (DOFs) solved with the model of the floor F2 ranged between 517 000 and 1 782 000 at low and high frequencies, respectively. The corresponding numbers of DOFs for the floor F3 were 243 000 and 1 178 000.

2.3. Post-processing. The radiated sound power P_{rad} was determined depending on the structure under study. In case of the floor F2, the sound power was computed by integrating the normal sound intensity I_{n} below the floor over the radiating plasterboard boundary S_{b}:

$$P_{\mathrm{rad}} = \int_{S_{\mathrm{b}}} I_{\mathrm{n}} dS \tag{12}$$

However, in case of the floor F3 where the radiating surface consisted of several surfaces, the sound power was estimated by integrating the sound pressure over a hemisphere boundary S_{h} with a 100 m radius:

$$P_{\mathrm{rad}} \approx \frac{1}{2\rho_{air}c_{air}} \int_{S_{\mathrm{h}}} pp^{*} dS \tag{13}$$

where the asterisk (*) denotes the complex conjugate [44]. Thus, the sound power was computed in a far-field condition applying exterior field calculation [53].

The simulated sound powers P_{rad} were converted into the normalised impact sound pressure level L_{n} by assuming perfectly diffused sound field in the receiving room as follows:

$$L_{\mathrm{n}} = 10\log\left(\frac{P_{\mathrm{rad}}}{P_0}\right) + 10\log\left(\frac{A_{\mathrm{ref}}}{A_0}\right) = L_W + 10\log\left(\frac{A_{\mathrm{ref}}}{A_0}\right) \tag{14}$$

where $P_0 = 10^{-12}\mathrm{W}$ is the reference sound power, and $A_0 = 10\,m^2$ and $A_{\mathrm{ref}} = 4\,m^2$ are the reference absorption areas [42,47].

In practical measurement situations, this ideal condition of a perfect diffuse sound field is not met. The assessment methods of the standard ISO 10140–3 [60] used to calculate the normalised impact sound pressure level L_{n} in the receiving room, inherently introduce uncertainty to the measurement results [61,62]. The uncertainty is at its highest in the low-frequency range, where the modal density of the receiving room is low.

2.4. Material properties. To describe the three-dimensional elastic behaviour in the structural domains of the simulations, information from the mechanical properties, i.e., the modulus of elasticity E, shear modulus G, and Poisson's ratio ν, was needed along with the material densities ρ. Describing orthotropic behaviour of a material requires determining nine independent elastic constants (E_{x}, E_{y}, E_{z}, G_{xy}, G_{xz}, G_{yz}, ν_{xy}, ν_{xz}, ν_{yz} where the subscripts x, y, and z denote the principal axes in a local cartesian coordinate system), whereas isotropic behaviour can be described with just two independent constants (namely E and G, or E and ν), in addition to the material densities. The principal axes were chosen to represent the longitudinal (x), transversal (y), and perpendicular (z) directions. The perpendicular axis (z) was for all materials in global vertical direction but the direction of x, and y depended on the part orientation in the floor (c.f. Fig. 5). Additionally, the loss factors η_s, and the poroacoustical properties were determined for the structural components and the glass wool, respectively.

Material properties provided by the product manufacturers have been presented in Table 1. The values were supplemented with information based on the values reported in the literature. In case of missing information such as the Poisson's ratios for elastomers, assumptions of the values were applied. Furthermore, the Poisson's ratios and (frequency-independent) loss factors of the plasterboards and the LVL products have not been presented by the manufacturers, but were estimated based on the reported values for plasterboards and plywood products in the refs. [29,44,59]. Properties presenting the thin carton layer of the thicker plasterboard were based on the information presented in the ref. [63]. These properties were applied only in the impact force simulations. The density of the carton was estimated based on its approximate thickness and on the presented mass proportions of gypsum core (95%) and the paper liner (5%) [64]. The dynamic modulus of elasticity of the elastomer product used to support the floors in the laboratory opening depends on its used capacity. To account for the loading of the elastomer by the floors F2 and F3, the respective dynamic moduli of elasticity were 0.83 and 1.3 MPa [65]. Additionally, when the structures of the laboratory opening were considered (see Sections 2.2.3 and 2.4), the steel frame and the sealing compounds around floors were constructed. The properties of the linen wool surrounding the rib slab were assumed to correspond to the properties of the glass wool. According to the data presented in Table 1, plasterboards, elastomers, steel frame and sealing compounds can be presented as linear isotropic elastic materials, but the wood-based products have clear orthotropic characteristics.

2.5. Impact sound insulation measurements. Impact sound insulation of the floors F1, F2, and F3 was measured in accordance with the standard ISO 10140–3 [60] in an accredited building acoustics laboratory (Eurofins Expert Services Oy, Espoo, Finland), in which the receiving room had a length of 3.9 m, width of 3.05 m, and height of 4.7 m. The experiments were performed to achieve 1/3-octave band results for the normalised impact sound pressure level L_{n} in the frequency range 50–5000 Hz. STM was used as an impact sound source in the ISI experiments in the five predetermined source positions as depicted in Fig. 6. Impact sound insulation measurements were carried out for all the floor construction stages F1–F3. In addition to the bare floor F2, the floor F1 was measured to determine the improvement of impact sound insulation ΔL of the floor covering installed on the floor F2. During the measurements, the reverberation time of the receiving room was also recorded.

2.6. Model validation

2.6.1. Simulations of impact force excitation. The impact force excitation model was validated by comparing the simulated impact force pulses to the experimental results presented in a previous study [73]. This was carried out by first simulating the previously measured impact force generated by the centre hammer of the STM in two source positions on the timber rib slab floors F6.0 and F9.0 [73] without and with the plasterboard layers on the rib slab. The floors F6.0 and F9.0 represented closely the bare floors F3 and F2 of the present study,

Table 1
Material properties of the studied floors provided by the manufacturers and supplemented with literature values. Assumed material parameters have been bolded.

Material	ρ [kg/m^3]	E_x [MPa]	E E_y [MPa]	E_z [MPa]	G_{xy} [MPa]	G G_{yz} [MPa]	G_{xz} [MPa]	ν_{xy} [-]	ν ν_{yz} [-]	ν_{xz} [-]	η_s [-]	R_f [Pa·s/m^2]
Plasterboard 12.5 mm[66]	672		1850*)			-			*0.25***)		*0.01***)	-
Plasterboard 15.5 mm[67]	994		4750*)			-			*0.25***)		*0.01***)	-
LVL deck 27 mm[68]	510	10500	2000	130	120	**600**	600	*0.25***)	*0.25***)	*0.25***)	*0.015***)	-
LVL beam 45 × 260 mm[68]	510	13800	130	430	600	**600**	380	*0.25***)	*0.25***)	*0.25***)	*0.015***)	-
Elastomer 12.5 mm[65]	256***)		0.83/ 1.3			-			**0.4**		0.18	-
Glass wool 95 mm[69,70]	13		-			-			-		-	6000
Carton (plasterboard 15.5 mm)[63]	*770*****)	*7440***)	*3470***)	*40***)	*2040***)	*99***)	*137***)	*0.15***)	*0.021***)	*0.008***)	-	-
Steel frame of the laboratory opening	*7800***)		*210000***)						*0.3***)		*0.0001***)	
Sealing compound	*1300***)		*0.6***)						**0.4**		**0.1**	

*) Average of longitudinal and transversal values. For plasterboard 12.5 mm, the values were 2100 and 1600 MPa [66], and for plasterboard 15.5 mm, 5000 and 4500 MPa [67].
**) Material values estimated based on the literature (italicised) [29,44,59,71,72].
***) Measured value for the specific material.
****) Material value estimated based on its approximate thickness (0.5 mm) and mass proportions of the plasterboard product [64].

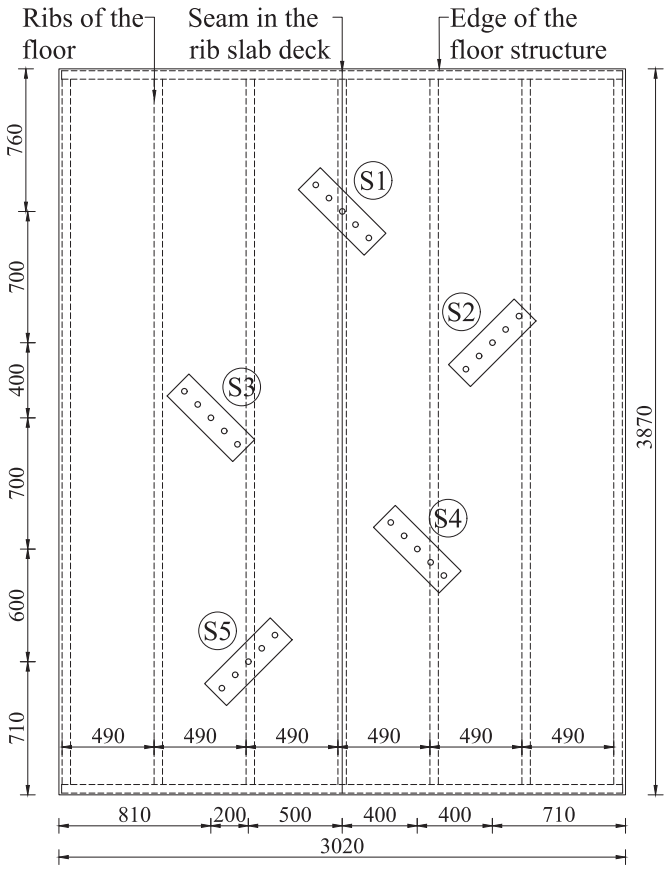

Fig. 6. ISO standard tapping machine (STM) positions S1–S5 on the floors. The presented dimensions (in millimetres) illustrate the area of the rib slab, spacing of the ribs, and the location of the centre hammer of the STM in different positions.

respectively. However, one difference between floors F9.0 and F2 was that the plasterboards of the floor F9.0 were attached to the surface of the rib slab by screwing without glue whereas in the case of F2 the plasterboards were both glued and screwed. This was considered in the impact force validation by modelling the contact between the plasterboards and the rib slab as frictional (LS-DYNA Keyword: *CONTACT_AUTOMATIC_SURFACE_TO_SURFACE [74]). The static and dynamic friction coefficients between the layers were assumed as 0.5. The chosen source positions were located at two extremes on the rib slab floor: the first lied at the top of the centre beam of the floors (S3 in ref. [73]), and the second between the beams (S4 in ref. [73]).

In the validation phase, the impact force simulations were performed with models presenting the geometry and the material properties of the previously measured floors. The material properties presented by the manufacturers corresponded mainly to those presented in Table 1, but due to the different LVL material provider dissimilar values for E_x (10100 MPa) of the LVL deck and G_{xz} of the LVL beams (440 MPa) were used in the validation [75]. Moreover, the carton surfaces of the plasterboards were applied. To simulate the impact force excitation driving the floors in the present study, the validated models were updated to present the geometry and boundary conditions of the floors F2 (without the suspended ceiling), and F3. Thus, it was presumed that the ceiling does not affect the impact force.

2.6.2. Simulations of impact sound radiation. The models for simulating the impact sound radiation of the floors F2 and F3 were validated by a comparison with the ISI measurement results. The validation was performed blindfolded, i.e., the simulation models of F2 and F3 were fully constructed before the ISI measurements were performed and the results were given to the authors. To ensure the exact order of the validation, the measurements were carried out (according to the plans given by the authors) as a purchased service. Moreover, the simulations and the measurements were performed with the same source positions S1–S5 (see Fig. 6). In case of the floor F1, the effect of the ΔL of the floor covering was taken from the measurement results and subtracted from the simulation results of the bare floor F2 as discussed in Section 2.2.1. The object of the validation was to find out how satisfactory the simulation procedure performs in predicting the normalised impact sound pressure level L_n of timber floors if only information of the construction and the used materials were known.

3. Results

3.1. Impact force excitation. Fig. 7 shows an example of the geometries and meshes around the impact area applied in the impact force model validation. Similarly as for the CLT slab in the previous study [49], it was

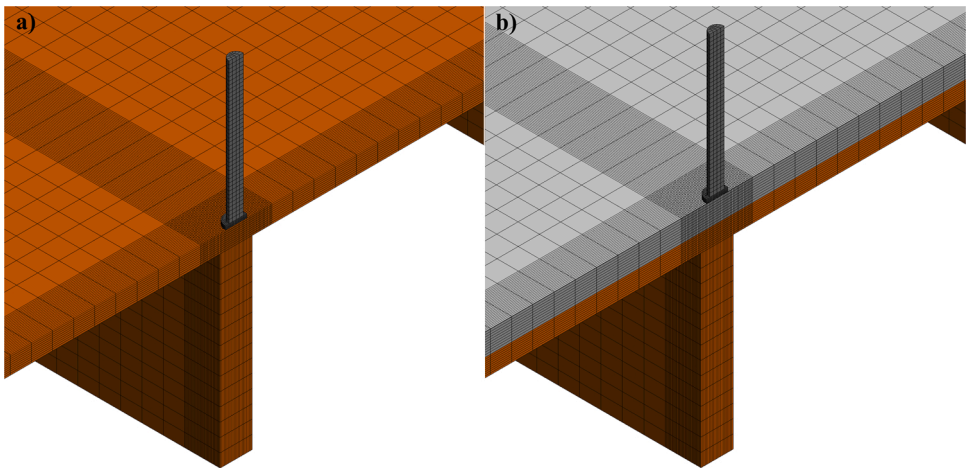

Fig. 7. Element mesh in the impact force model validation at the source position at the top of the centre beam for the floors: a) F6.0 and, b) F9.0.

noticed that the local properties of the rib slab were important for the impact force and there was no need to simulate the behaviour of the entire floor during the collision. In other words, partial models of the floor resulted practically to the same impact forces than the models with the entire floor. This occurs due to the short duration of the impact force pulse: waves do not have enough time to reflect from the floor boundaries to the impact area. Thus, we applied symmetry and partial models of the floors in the impact force computations. The mesh below the impact area consisted of ten element layers per plasterboard or LVL deck, and the beams were meshed with 14 element layers in the vertical direction. The carton layer of F9.0 had a mesh consisting of a single element layer. The carton layer was applied since it affects the impact force pulse by lowering the peak value of the pulse. Around the impact area, a 100 × 100 mm^2 area had a mesh with 2 mm element lengths in horizontal directions. Elsewhere the element length was set to 30 mm.

The simulated impact force results were compared with the measurement results presented in ref. [73]. Fig. 8 illustrates the simulated and measured impact force pulses $F(t)$ in the time domain (left column), and the magnitudes of their single-sided amplitude spectra F_n (right column). Note that the results partly overlap. Furthermore, Table 2 shows the key parameters describing the excitation in scalar values, i.e.,

Table 2
Impact force model validation: Comparison of the peak value of the force F_{peak}, low-frequency force F_{lf}, mechanical impulse I, and length of the force pulse T_{pulse} determined for the measured and simulated force pulses. The measurement results from the experiments [73] represent averages based on all the measured force pulses at the respective situation.

Floor and source position	Measured (M)/ Simulated (S)	F_{peak} [N]	F_{lf} [N]	I [Ns]	T_{pulse} [ms]
F6.0, at top of the beam	M	1329	2.96	0.74	1.24
	S	1340	3.00	0.75	1.00
F6.0, at between the beams	M	610	2.30	0.57	2.10
	S	876	1.95	0.49	1.17
F9.0, at top of the beam	M	1835	2.48	0.62	0.85
	S	2083	2.86	0.72	0.67
F9.0, at between the beams	M	1566	2.22	0.56	0.93
	S	1982	2.61	0.65	0.65

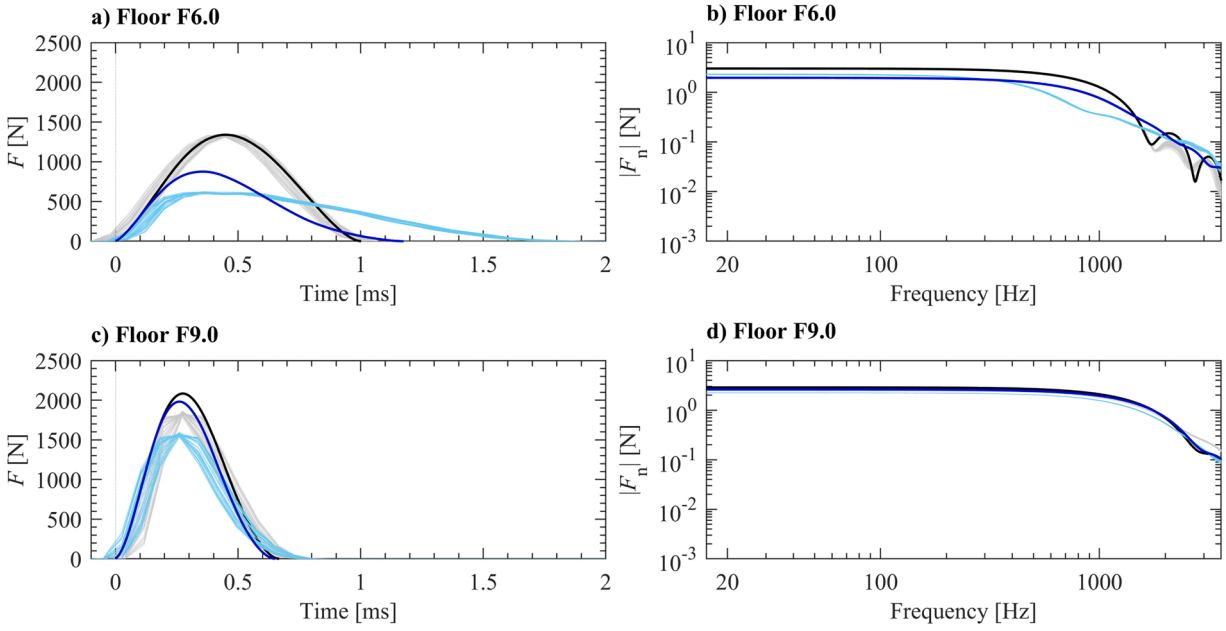

Fig. 8. Impact force model validation: Simulated impact force pulses $F(t)$ and magnitudes of their single-sided amplitude spectra F_n (black (at top of the beam) and blue (at between the beams) lines) and the corresponding measurement results from the experiments [73] (thin grey (at top of the beam) and light blue (at between the beams) lines).

peak value of the force F_{peak}, low-frequency force F_{lf}, mechanical impulse I, and length of the force pulse T_{pulse}. According to the results, the validation model closely predicted the measured impact force pulse on the floor F6.0 at the top of the centre beam but at between the beams, the simulation underestimated the T_{pulse} and I, and overestimated the F_{peak}. These issues can also be seen from the frequency domain results: the simulated force spectrum was in a wide frequency range nearly equivalent with the measurement results at the top of the beam but at between the beams there were prominent discrepancies between the simulated and measured spectra around mid-frequencies. In case of the floor F9.0, similarity of the simulated and measured results was rather good although the computational model slightly overestimated the F_{peak} and I. This again can be seen as a resemblance of the results in the frequency domain.

Probable causes for the deviation between the simulation and measurement results of the impact force are the local inhomogeneities in the measured rib slab and differences in the actual material properties in comparison with those applied in the simulations [49]. Additionally, in case of the floor F9.0, the exact friction coefficients were not known for the contact between the plasterboards and the rib slab. However, the best available information from the properties of the floors led to acceptable equivalency between the results. Thus, the impact force model was regarded as valid to be applied in predicting the impact force excitations of the floors F2 and F3 of this study.

The validated impact force models were modified to correspond with the timber slabs of the floors F2 and F3 and applied to compute their

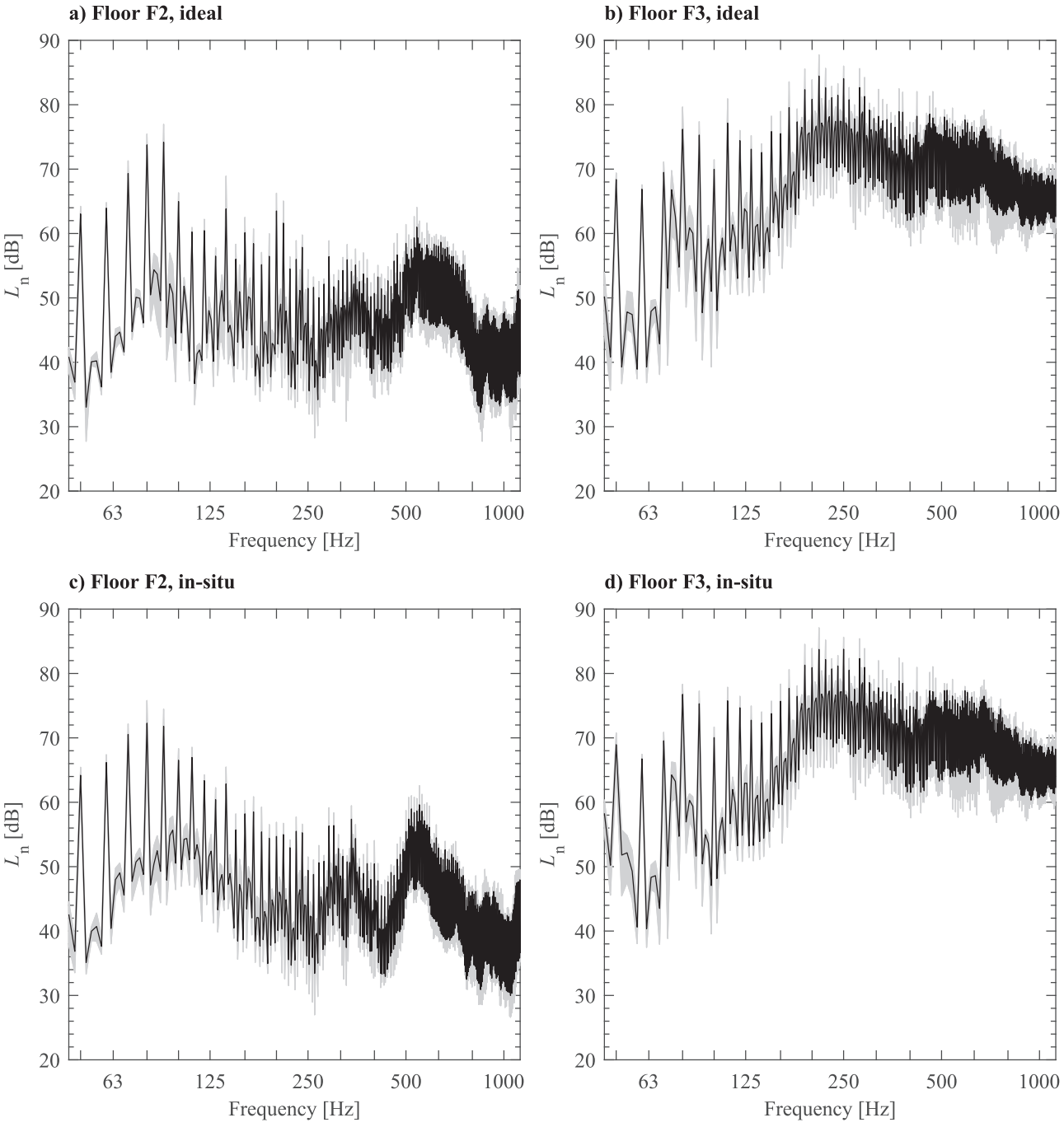

Fig. 9. Simulated narrow-band normalised impact sound pressure levels L_n for the floors F2 (a, c) and F3 (b, d). Spatially averaged results have been illustrated with black lines and the grey areas show the range of results caused by different source positions.

impact force excitations at the source positions S1–S5 following the same procedure. The postprocessed excitation results for the floors have been shown in Figs. A1 and A2 in the appendix A of this paper. In the ISI simulations, the solved magnitude and phase spectra of the repeated force pulses were applied to excite the studied floors in the frequency domain analyses.

3.2. Simulation and measurement results. Fig. 9 presents the simulation results for the normalised impact sound pressure level L_n in case of the ideal and in-situ models of the floors F2 and F3. The figure presents the spatially averaged narrow-band results (2 Hz frequency resolution) in the frequency range covering the 1/3-octave bands from 50 to 1000 Hz together with the ranges describing the effect of the variation on the L_n caused by different source positions. The highest low-frequency values for the L_n occurred at 80 Hz both for the floors F2 and F3. The behaviour of the structures at this frequency has been illustrated in Fig. 10 where the displacement of the structural domains and the sound pressure in the acoustical domains as well as the sound radiation can be seen.

Laboratory measurement results for the L_n have been presented in Fig. 11 for the floors F1–F3 and in case of the ΔL of the floor covering. The results for the L_n represent the energy averaged levels based on all the source positions in the 1/3-octave bands 50 to 5000 Hz. Additionally, Table 3 presents the measurement results as SNQs $L_{n,w}$, C_I, and $C_{I,50-2500}$ calculated according to the standard ISO 717–2 [76]. According to the results, the $L_{n,w}$ improved from 91 dB to 66 and 60 dB, when the floor F3 was constructed to F2 and F1.

To ease comparison of the measurement and simulation results, Fig. 12 presents the 1/3-octave band integrated simulation results of the normalised impact sound pressure levels L_n for the floor construction stages F1–F3. In addition, the figure illustrates the measurement results for the L_n in the frequency range 50–1000 Hz. As stated in the description of the procedure (see Section 2.2.1), the only difference between the results for the floors F1 and F2 is that in the case of floor F1 the measured ΔL of the floor covering (Fig. 11b) has been taken into account. The effect of the floor covering was the same for measurements and simulations. Hence the similar correspondence with the simulation and measurement results of the floors F1 and F2. According to the results presented by the Fig. 12, the *ideal* simulation results deviated from the measurement results by 0.5–7.0 dB, 0.4–6.8 dB and 0.6–11.0 dB, for the floors F1, F2 and F3, respectively. The respective deviations of the *in-situ* simulation results from the measurement results were 1.0–8.8 dB, 0.9–8.2 dB and 1.0–11.1 dB.

To further investigate the equivalency of the results, differences between the measured and simulated L_n were calculated in 1/3-octave bands for each computation and measurement combination of the floors F2 and F3 and for all source positions (Fig. 13). According to the results, the equivalency of the measurement and simulation results seemed to be at best when the floors were excited at the source positions S1, S4, and S5. On the other hand, the differences were at the largest when the source position lied between the ribs, i.e., at the positions S2

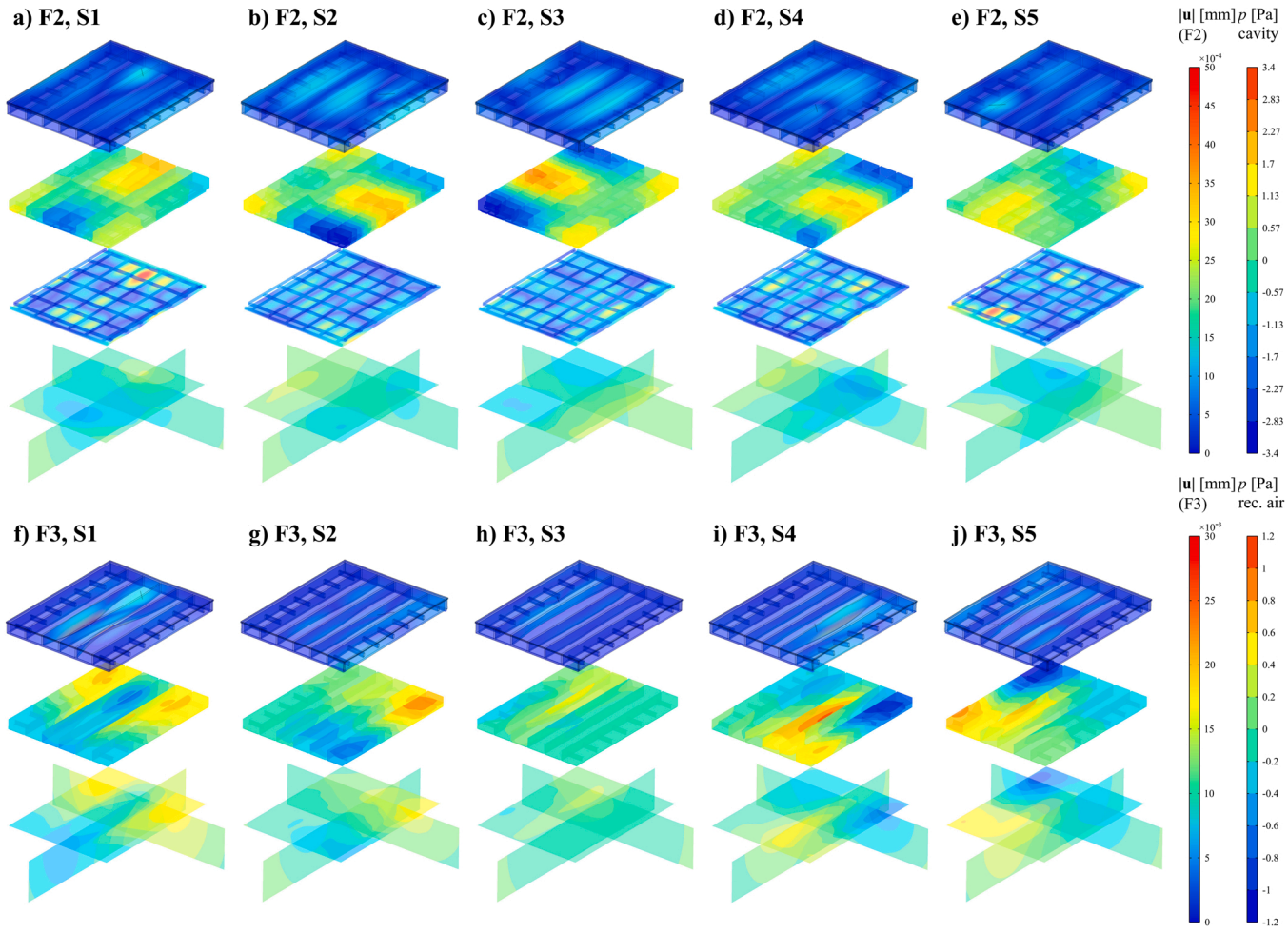

Fig. 10. Simulation results at 80 Hz as exploded views for the ideal floors F2 (a-e) and F3 (f-j) excited at the source positions S1–S5. The upper row (a-e) presents the displacement magnitude $|\mathbf{u}|$ of the rib slab, the sound pressure p in the floor cavity, the $|\mathbf{u}|$ of the suspended ceiling, and the p in the receiving airspace in case of the floor F2 from top to bottom. The lower row (f-j) presents the $|\mathbf{u}|$ of the rib slab, and the p between the ribs and in the receiving airspace. The displacements have been shown in millimetres and sound pressures both in air cavity and in the receiving airspaces in Pascals.

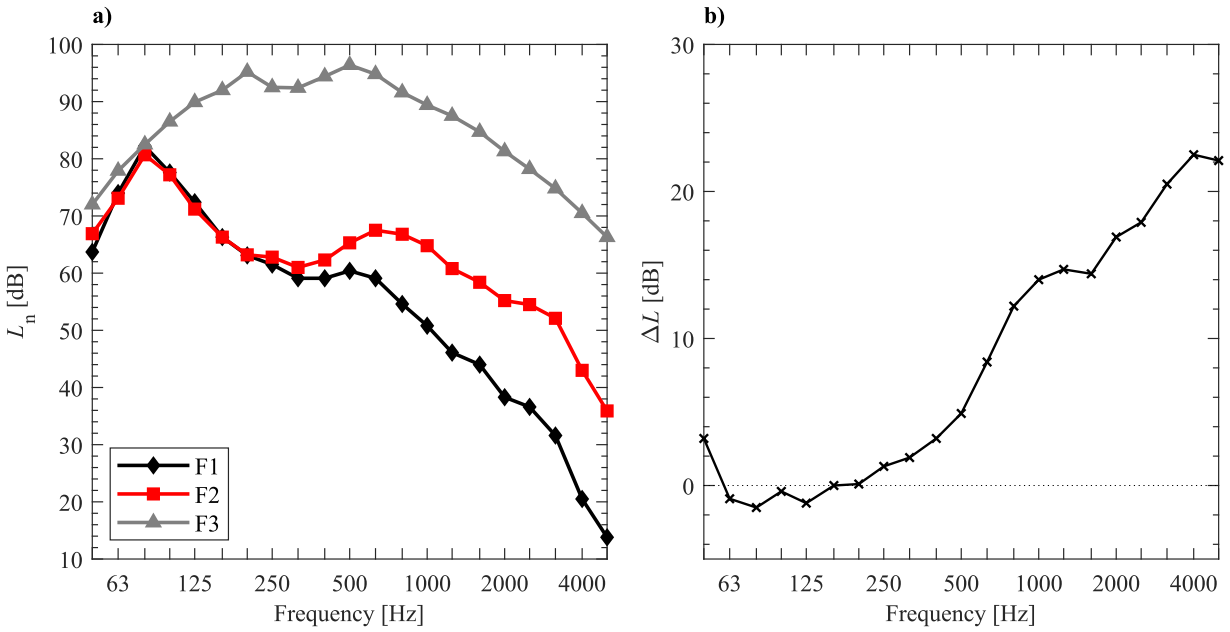

Fig. 11. Measurement results for the normalised impact sound pressure levels L_n in 1/3-octave bands for all the studied floors F1–F3 (a), and for the ΔL of the floor covering (b).

Table 3
Measurement results in single-number quantities according to ISO 717–2 [76].

Floor	$L_{n,w}$	C_I	$C_{I,50\text{-}2500}$
F1	60 dB	4 dB	9 dB
F2	66 dB	-1 dB	3 dB
F3	91 dB	-2 dB	-2 dB

and S3. One possible explanation for the latter is that the impact force excitation is less well simulated for these source position, as observed based on Fig. 8.

3.3. Effect of the ceiling contacts on the results. The abovementioned simulation results for the floors F1 and F2 involved models where the contacts between the supporting structures of the ceiling were regarded as point and line contacts. The effect of including the no separation boundary constraints between the supporting structures has been illustrated in Fig. 14 for the floor F2. According to the results, addition of the no separation constraints increased the L_n levels in a broad frequency range but decreased the levels in the low frequencies (Fig. 14). This kind of behaviour implies for stiffening of the ceiling suspension system which can be considered as an expected result from the analysis. Additionally, it was observed that including the constraints decreased the variation of the L_n with respect to the source position.

4. Discussion

4.1. Model applicability and findings. The measurement results presented in Fig. 11a illustrate how the ISI of the measured floor gradually improved when the floor plasterboards, the suspended ceiling and the floor covering were added to the bare rib slab. According to the results, the plasterboards, and the suspended ceiling minorly affected the ISI at the 1/3-octave bands 50–80 Hz but above this range their improving effect was evident. Thus, the comparison of the results for the floors F2 and F3 indicates for a resonance frequency of the suspended ceiling at the 80 Hz frequency band. The improvement of ISI achieved with the floor covering began from 250 Hz band (see Fig. 11b). The resulting ΔL can be regarded modest in comparison with the results for a similar floor covering on a concrete floor (for example, see [77]). This result is in line with the findings of a recent paper [54].

Based on the SNQs presented in Table 3, it could be possible to use the floor F1 as an apartment floor at least in some European countries (c. f. [6]). The SNQs $L_{n,w}$, $L_{n,w} + C_I$, and $L_{n,w} + C_{I,50\text{–}2500}$ for the floor F1 were fully determined based on the L_n in the frequencies below 200 Hz. In case of the floor F2, the SNQs $L_{n,w} + C_I$, and $L_{n,w} + C_{I,50\text{–}2500}$ were determined by the results below 1000 Hz. Thus, the chosen frequency range covering the 1/3-octave bands 50–1000 Hz can be regarded justified for the L_n simulations.

The L_n simulations were performed with a 2 Hz frequency spacing in the abovementioned frequency range (see Fig. 9). Based on the narrow-band results, it is evident that the excitation generated by the STM induced large peaks to L_n on multiples of 10 Hz. This occurs due to the excitation model [49,52] applied to describe the continuous operation of the apparatus but the behaviour also corresponds with the findings presented in the research literature for real STMs [52]. The prominent peaks dominate the 1/3-octave band results for the L_n, but especially in the low-frequency range the results between the multiples affect the band integrated results as well. However, in the high-frequency range, an acceptable accuracy could have been achieved by performing the computations only at the multiples.

Correspondence between the simulation and measurement results in 1/3-octave bands was the best with the floors F1 and F2 (see Fig. 12). In case of these floors, the low-frequency simulation results were lower than the measurement results. The most prominent differences between the simulation and measurement results, where the simulation results deviated from the measurement results around 5 to 9 dB, occurred around 80 Hz and 500 Hz bands. In case of the floor F3, the simulation results were considerably lower than the measured ones in the entire frequency range 50–1000 Hz. Although the simulated frequency range did not cover all the frequencies needed in the standardised SNQ rating, the discrepancies between the measurement and simulation results for the floors F1 and F2 correspond to 0–2 dB differences in $L_{n,w}$ and $L_{n,w} + C_I$, and 3–4 dB differences in $L_{n,w} + C_{I,50\text{–}2500}$ if values beyond the studied frequency range are omitted. The larger scale for the latter is caused by the differences seen in the 80 Hz frequency band for the floors F1 and F2. In case of the bare rib slab (floor F3), the simulations underestimated the normalised impact sound pressure levels, and the corresponding differences were 4–5 dB for all the abovementioned

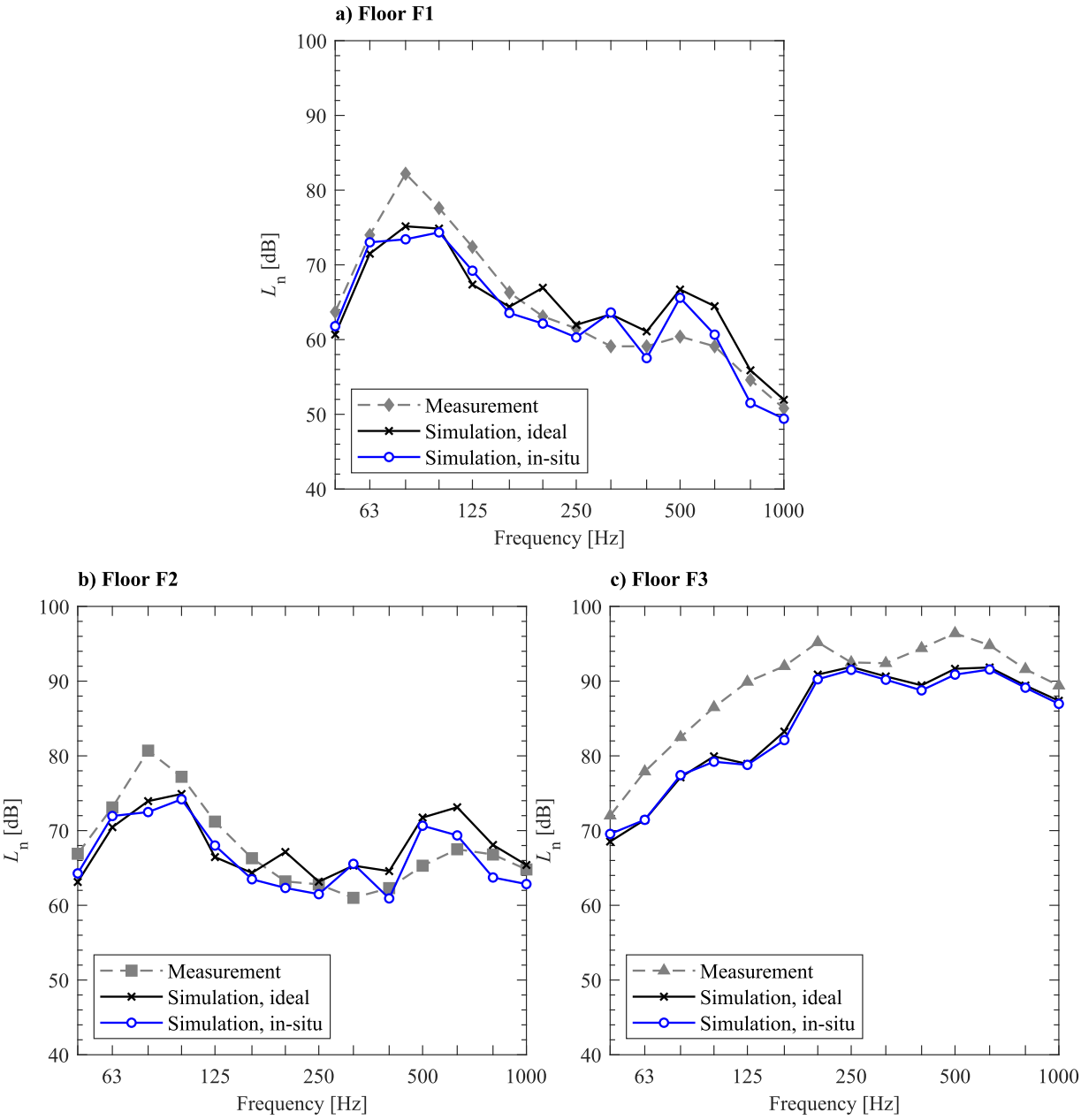

Fig. 12. Simulated and measured 1/3-octave band integrated normalised impact sound pressure levels L_n for the floors F1–F3.

SNQs. The prediction errors were larger than for the timber rib slab presented by Wang et al. [47].

Comparison of the simulation and measurement results indicates for probable reasons for the differences. The two prominent peaks in the mid-frequency simulation results at the 250 Hz and 630 Hz bands for the floor F3 appeared to be shifted in adjacent frequency bands in comparison with the measurement (see Fig. 12c). This implies that the orthotropic material parameters for the LVL applied in the simulations do not fully correspond to those of the measured floor. Moreover, since the normalised impact sound pressure levels were underestimated by the simulations, it is also possible that the mass or the loss factors of the floor F3 (or both) were overestimated. These level differences were also affected by the probably too low impact force spectra predicted for the STM positions between the beams. These issues highlight the common problem with all the deterministic models, including FEM, when the material properties are variable. Additionally, it must be noted that the applied simulation procedure does not take into account the mode coupling between the floor and the receiving room, which e.g. Wang et al. [47] has found to improve the correspondence between measurement and simulation results in case of a rib slab. These are probable causes leading to differences between the results of the floors F1 and F2, as well. Furthermore, it raises a question of how the material parameters or the modelling procedures affect the simulation results.

Since the ideal and in-situ conditions resulted in rather similar L_n levels for the floor F3, it seems that the result for the rib slab was quite insensitive for small changes in boundary conditions. Interestingly, however, including the in-situ boundary conditions to the simulation model improved the overall consistency of the results for the floors F1 and F2 (see Fig. 12a-b). It was also seen that the addition of no separation constraints to the supporting structures of the ceiling affected the results greatly (see Fig. 14). This suggests that the result can be sensitive to modelling inaccuracies. Thus, it seems justified to model the suspended ceilings in detail to improve the accuracy of the simulation. However, as seen from the differences illustrated in Fig. 13, it is obvious that the accuracy of the simulation results is dependent on the source position.

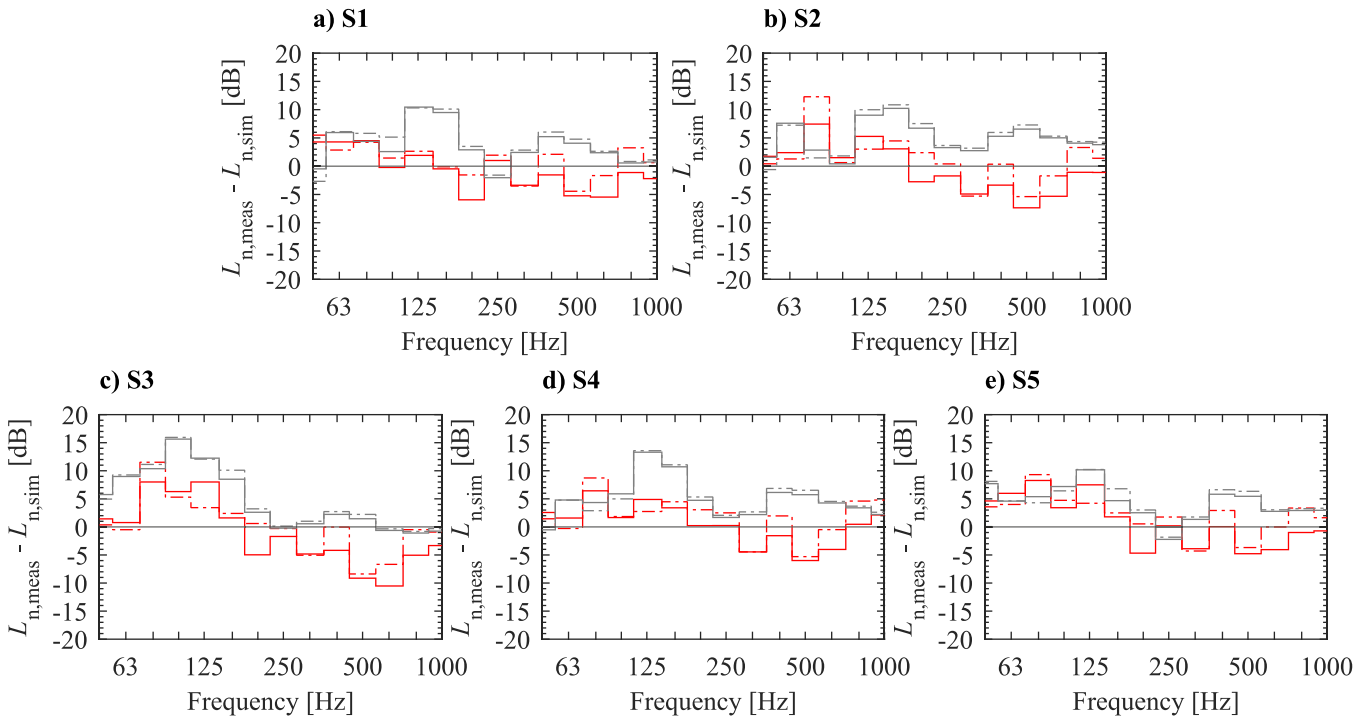

Fig. 13. Differences between the measurement ($L_{n,meas}$) and simulation ($L_{n,sim}$) results in 1/3-octave bands for the floors F2 and F3 when the STM was located at source positions S1–S5. Differences between the measured and simulated L_n for the floor F2 have been presented in red, and for the floor F3 in grey colour. Comparison with the ideal models have been depicted with solid lines (-), and with dash-dotted lines (-.) for in-situ models.

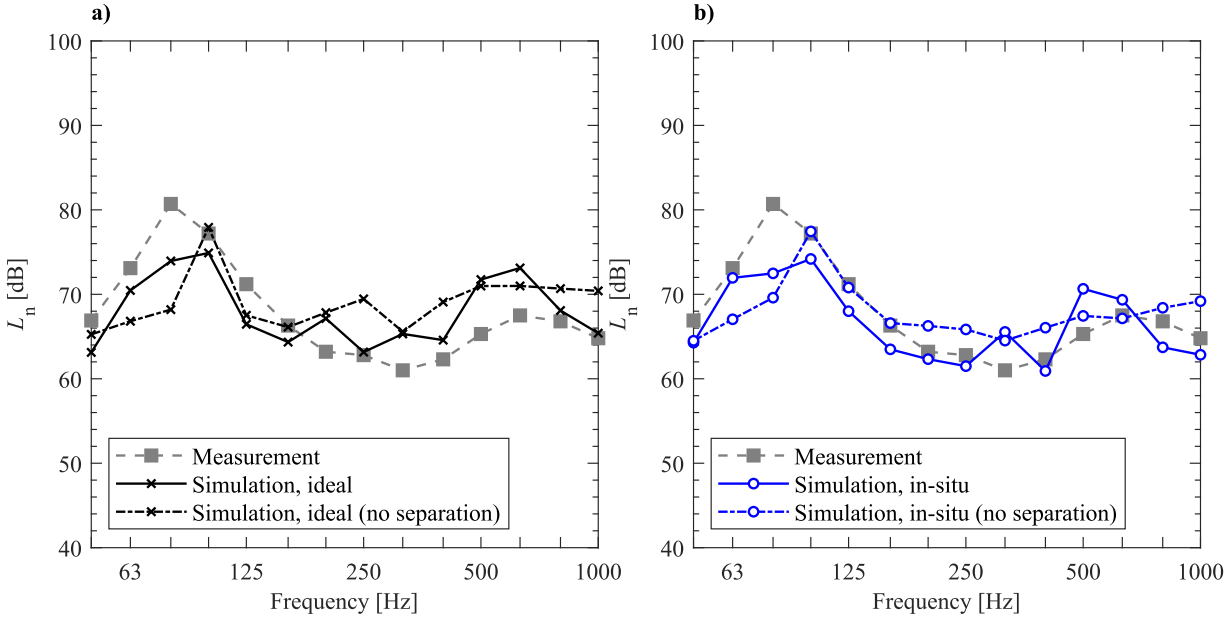

Fig. 14. The effect of including the no separation boundary constraints to the supporting structures of the ceiling. Comparison of the ideal (a) and in-situ (b) simulation results with the measurements in case of the floor F2.

4.2. Limitations and need for further research. The applied model to compute the impact force pulse on the floors has previously been validated to model the excitation on a CLT slab [49]. According to the comparison of the simulation and measurement results in Fig. 8, the model was capable of predicting the impact force pulses and the force spectra on the rib slabs as well, despite minor discrepancies. However, it must be noted that the measurement data used in the validation concerned a previous study rather than the present one. Furthermore, the applied post-processing method to present continuous operation of the STM leads to an ideal excitation spectrum with a 2 Hz frequency resolution [52]. This assumption introduces uncertainty especially to the low-frequency results if the repetition time between the impacts caused by the hammers of the STM deviate largely from the ideal.

The performed simulations mainly utilised data provided by the product manufacturers instead of measured material properties of the actually studied floors. This starting point corresponds with research and product development tasks where similar source information represents the best available data for the analysis. However, because of the

chosen method, it remains unclear whether the actual material properties would improve the equivalence between the simulation and measurement results for the ISI. Thus, it is highly recommended that a study of this type is repeated with known material data of measured floors. This would also bring insight into the possible modelling inaccuracies. The modelling was performed according to the best current knowledge of the authors but due to the complexity of the studied structures inaccuracies can occur. These inaccuracies can be related to the mesh density, boundary conditions and contacts/constrains between parts, to give examples. Due to the deterministic nature of the FEM simulations, changing the parameters will have an effect on the results. Another point of view is that it is not known how sensitive the simulation model (or even the measurement result) is for different kind of changes in the timber floors. These changes include variations in materials, dimensions, and joints, to give examples. For this reason, it is recommended that a sensitivity analysis for the simulations is performed.

And finally, although the impact force excitation models were cost-efficient and solved the tasks presented here within half an hour per model with 2 CPU cores, the simulation of the sound radiation of the floor was rather time-consuming. Due to the non-symmetrical matrices, solving the model of the floor F2 for the five source positions took approximately one week with 16 CPU cores. Thus, it is obvious that further studies are needed to speed up the computations. First of all, application of less expensive element types such as beam and plate elements instead of full solid elements would be beneficial, e.g., as previously applied by Wang et al. [47]. Secondly, techniques to compute the impact sound radiation of the floors with a coarser frequency resolution outside the low frequencies (for example, as in ref. [47]) should be adopted.

5. Conclusions

This paper studied the ability of FEM simulations to predict impact sound insulation (ISI) of a full-scale timber floor. The simulation procedures were applied to find out whether the currently known methods can be utilised to imitate ISI laboratory measurements of timber floors driven by an ISO standard tapping machine (STM). From another point of view, it was studied how the results for the normalised impact sound pressure level L_n differ when in-situ boundary conditions and constraints are considered instead of idealised models. These are especially important questions for the acoustical engineers and researchers working with the product development of timber construction industry.

Methodologically, the questions were answered by performing blindfolded validations of FEM models for the floor without covering (F2) and for the bare rib slab (F3) in a frequency range 50–1000 Hz, using mainly the data provided by the product manufacturers to describe the behaviour of the materials used in the structures. This corresponds to the bases of the researchers or product developers carrying out predictions in a similar task since thorough experimental validations cannot always be performed. The model for the floor F2 was further applied together with the measurement result of ΔL of the floor covering to simulate the L_n of the full floor F1. The study indicates that the applied procedure results in a 0.4–8.8 dB correspondence between the simulated and measured L_n for the full timber floor (F1) and the floor without covering (F2) and can predict their SNQs with 0–2 dB ($L_{n,w}$ and $L_{n,w} + C_I$), and 3–4 dB ($L_{n,w} + C_{I,50–2500}$) accuracies even not knowing the actual material properties. In case of the bare rib slab (F3), the simulations underestimated the measured L_n by 0.6–11.1 dB and the SNQs $L_{n,w}$, $L_{n,w} + C_I$, and $L_{n,w} + C_{I,50–2500}$ by 4 to 5 decibels. It was noticed that including the in-situ conditions to the model improved the overall accuracy of the simulations of the full floors. The discrepancies between the results were probably caused by differences in the actual and simulated material properties and possibly by modelling inaccuracies.

Statements of originality

The results have not been published previously and the manuscript has not been submitted to any other journal.

CRediT authorship contribution statement

Jesse Lietzén: Writing – original draft, Visualization, Methodology, Investigation, Formal analysis, Conceptualization. **Ville Kovalainen:** Writing – review & editing, Methodology, Conceptualization. **Mikko Kylliäinen:** Writing – review & editing, Methodology. **Sami Pajunen:** Writing – review & editing, Supervision, Methodology, Funding acquisition.

Declaration of Competing Interest

The authors declare that they have no known competing financial interests or personal relationships that could have appeared to influence the work reported in this paper.

Data Availability

All relevant data needed to reproduce the research has been given in the article.

Acknowledgements

This paper was written within the Doctoral School in Industrial Timber Construction of Tampere University. Authors are grateful for Metsä Wood, Saint-Gobain Finland/Gyproc, Saint-Gobain Finland/Isover, and Christian Berner for the donated materials to this research. The authors would also like to express their gratitude to Mr Mika Lojander and Mr Ville Joensuu from Eurofins Expert Services Oy for cooperation and performing the laboratory measurements of impact sound insulation.

Appendix A

The simulated and post-processed results for the repeated impact force excitation of the floors F2 and F3 at the source positions S1–S5 have been illustrated by the Figs. A1 and A2, respectively. The figures present the excitation generated by the STM in time and frequency domains.

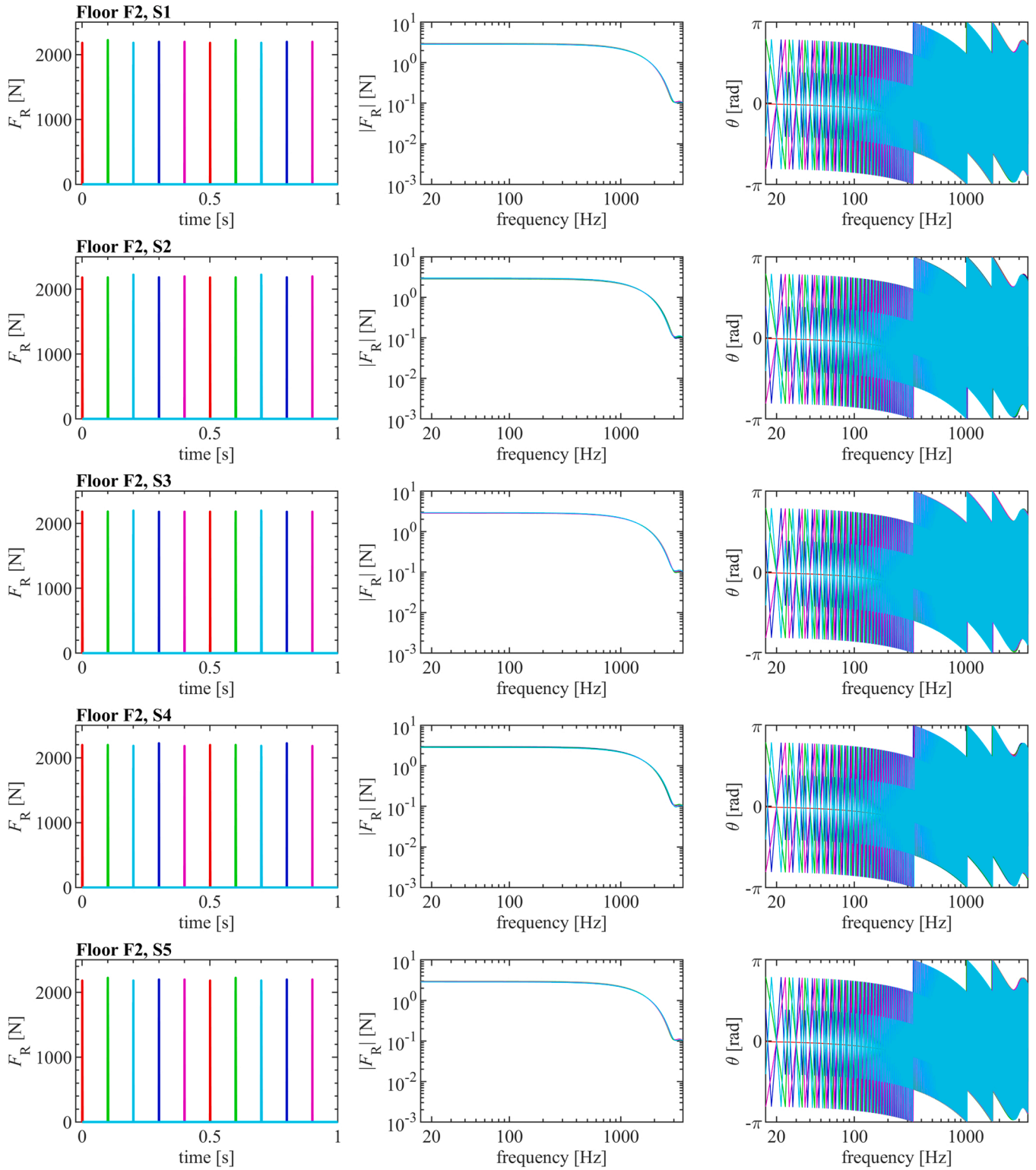

Fig. A1. Simulated and post-processed results for the impact force excitation generated by the STM on the floor F2 at the source positions S1–S5 (in rows). Time history of the repeated force pulses $F_R(t)$ have been shown in the left column whereas magnitude and phase of the spectrum of repeated force pulses $|F_R(t)|$ and θ, respectively, have been shown in the centre and right columns.

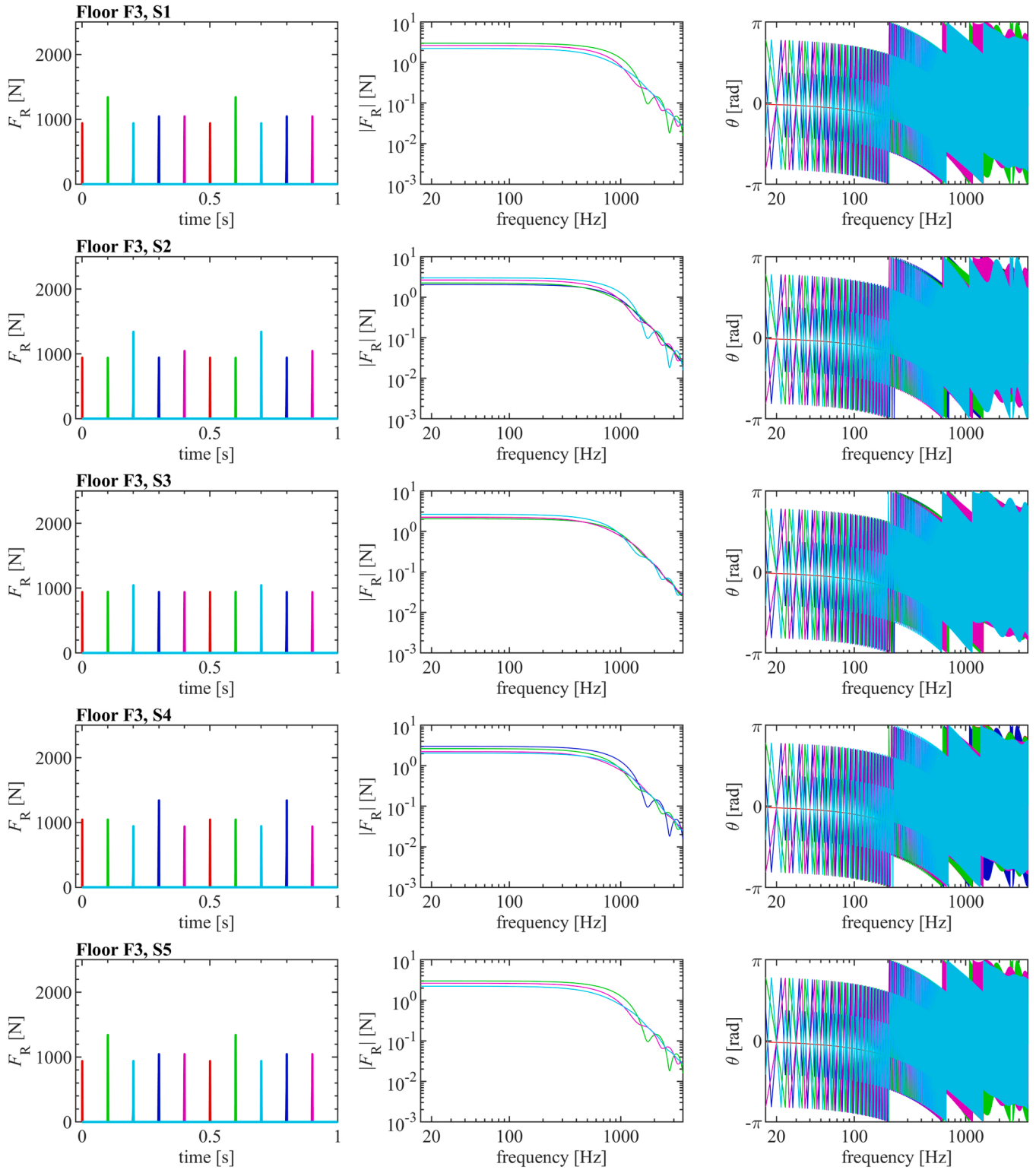

Fig. A2. Simulated and post-processed results for the impact force excitation generated by the STM on the floor F3 at the source positions S1–S5 (in rows). Time history of the repeated force pulses $F_R(t)$ have been shown in the left column whereas magnitude and phase of the spectrum of repeated force pulses $|F_R(t)|$ and θ, respectively, have been shown in the centre and right columns.

.

References

[1] EN ISO 12354–2. Building acoustics – Estimation of acoustic performance of buildings from the performance of elements – Part 2: Impact sound insulation between rooms. Brussels: European Committee for Standardization; 2017.

[2] Brunskog J, Hammer P. Prediction Models of Impact Sound Insulation on Timber Floor Structures; A Literature Survey. Build Acoust 2000;7:89–112.

[3] Forssén J., Kropp W., Brunskog J., Ljunggren S., Bard D., Sandberg G., et al. Acoustics in wooden buildings – State of the art 2008. Vinnova project 2007–01653. SP Rapport 2008:16. vol. XV. Stockholm, Sweden: SP Technial Research Institute of Sweden; 2008.

[4] ISO 10140–5. Acoustics – Laboratory measurement of sound insulation of building elements – Part 5: Requirements for test facilities and equipment. Geneva: International Organization for Standardization; 2021.

[5] ISO 16283-2. Acoustics – Field measurement of sound insulation in buildings and of building elements – Part 2: Impact sound insulation. Geneve: International Organization for Standardization; 2015.

[6] Rasmussen B. Sound insulation between dwellings - Comparison of national requirements in Europe and interaction with acoustic classification schemes. Proceedings of the International Congress on Acoustics, Aachen, Germany: 2019, p. 5102–5109. https://doi.org/10.18154/RWTH-CONV-239983.

[7] Asakura T. Prediction of vibroacoustic transmission characteristics through double-plate floor structures by using finite-difference time-domain analysis. Acoust Sci Technol 2019;40:344–55. https://doi.org/10.1250/ast.40.344.

[8] Asakura T. Numerical investigation of the sound-insulation effect of a suspended ceiling structure with arrayed Helmholtz resonators by the finite-difference time-domain method. Appl Acoust 2021;172:107601. https://doi.org/10.1016/j.apacoust.2020.107601.

[9] Cho T. Vibro-acoustic characteristics of floating floor system: The influence of frequency-matched resonance on low frequency impact sound. J Sound Vib 2013;332:33–42. https://doi.org/10.1016/j.jsv.2012.07.047.

[10] Cho T. Experimental and numerical analysis of floating floor resonance and its effect on impact sound transmission. J Sound Vib 2013;332:6552–61. https://doi.org/10.1016/j.jsv.2013.08.011.

[11] Kim TM, Kim JT, Kim JS. SEA-FEM hybrid analysis for predicting Inter-floor impact noise. Appl Acoust 2018;129:397–407. https://doi.org/10.1016/j.apacoust.2017.08.025.

[12] Kim TM, Kim JT, Kim JS. Effect of structural vibration and room acoustic modes on low frequency impact noise in apartment house with floating floor. Appl Acoust 2018;142:59–69. https://doi.org/10.1016/j.apacoust.2018.07.034.

[13] Park S, Kim H. Development of analytical impact force models for floor impact vibration and acoustic numerical analysis. Appl Sci 2016;6:120. https://doi.org/10.3390/app6050120.

[14] Jean P, Siwiak H, Joubert G. A decoupled vibro-acoustic development of FEM: Application to laboratory modelling. Build Acoust 2006;13:83–98. https://doi.org/10.1260/135101006777630463.

[15] Vastiau J., Van hoorickx C., Reynders E. Numerical and experimental investigation of the narrow-band impact sound insulation of layered floors. Proceedings of Inter-Noise 2022, Glasgow, Scotland: 2022.

[16] Bard D, Sonnerup J, Sandberg G. A Finite Element Solution of Structure-Borne Sound Attenuation for a Lightweight Timber Floor. Build Acoust 2008;15:137–52.

[17] Negreira J, Sjöström A, Bard D. Low frequency vibroacoustic investigation of wooden T-junctions. Appl Acoust 2016;105:1–12. https://doi.org/10.1016/j.apacoust.2015.11.016.

[18] Shen X., Hopkins C. Experimental validation of a finite element model for a heavy impact from the standard rubber ball on a timber floor. Proceedings of International Congress on Acoustics ICA 2019, Aachen, Germany: 2019, p. 1271–7.

[19] Shen X., Hopkins C. Prediction of maximum fast time-weighted velocity levels from a rubber ball impact on a timber floor. Proceedings of Forum Acusticum 2020, Lyon, France: 2020, p. 1651–5.

[20] Shen X., Hopkins C. Low-frequency vibration of a timber joist floor section connected by metal screws: experimental validation of FEM model. Proceedings of Inter-Noise 2022, Glasgow, Scotland: 2022.

[21] Negreira J., Bard D. Modelling of the tapping machine for finite element prediction tools -Preliminary parametric studies. Proceedings of International Congress on Acoustics, Buenos Aires, Argentina: 2016, p. 132.

[22] Persson P, Flodén O. Effect of material parameter variability on vibroacoustic response in wood floors. Appl Acoust 2019;146:38–49. https://doi.org/10.1016/j.apacoust.2018.10.034.

[23] Filippoupolitis M., Hopkins C., Völtl R., Schanda U., Mahn J., Krajci L. Experimentally validated finite element models for the modal response of a solid timber floor formed from dowel–connected joists. Proceedings of Forum Acusticum 2014, vol. 55, Krakow, Poland: 2014.

[24] Filippoupolitis M, Hopkins C, Völtl R, Schanda U, Mahn J, Krajči L. Structural dynamics of a dowelled-joist timber floor in the low-frequency range modelled using finite element simulation. Eng Struct 2017;148:602–20. https://doi.org/10.1016/j.engstruct.2017.07.009.

[25] Qian C, Ménard S, Bard D, Negreira J. Development of a vibroacoustic stochastic finite element prediction tool for a CLT floor. Appl Sci 2019;9:1–25. https://doi.org/10.3390/app9061106.

[26] Qian C, Ménard S, Bard-Hagberg D, Kouyoumji JL, Negreira J. Calibration of the ISO tapping machine for finite-element prediction tool on a wooden-base floor. Build Acoust 2019;26:157–67. https://doi.org/10.1177/1351010×19855227.

[27] Bard D., Negreira J., Guigou Carter C., Borello G., Kouyoumji J., Speranza A., et al. Modelling prerequisites – FEM/SEA Impact and Airborne Sound. Silent Timber Build, report no STB01 WG1. RISE Research Institutes of Sweden AB; 2017.

[28] Bolmsvik Å, Brandt A. Damping assessment of light wooden assembly with and without damping material. Eng Struct 2013;49:434–47. https://doi.org/10.1016/j.engstruct.2012.11.026.

[29] Bolmsvik Å, Linderholt A, Brandt A, Ekevid T. FE modelling of light weight wooden assemblies - Parameter study and comparison between analyses and experiments. Eng Struct 2014;73:125–42. https://doi.org/10.1016/j.engstruct.2014.04.028.

[30] Flodén O, Negreira J, Persson K, Sandberg G. The effect of modelling acoustic media in cavities of lightweight buildings on the transmission of structural vibrations. Eng Struct 2015;83:7–16. https://doi.org/10.1016/j.engstruct.2014.10.037.

[31] Hopkins C., Filippoupolitis M., Ferreira N., Völtl R., Schanda U., Mahn J., et al. Vibroacoustic finite element modelling of the low-frequency performance of a solid timber floor formed from dowel-connected joists. Proceedings of Inter-Noise 2016, Hamburg, Germany: 2016, p. 1115–22.

[32] Buchschmid M., Kohrmann M., Müller G., Schanda U. Vibroacoustic Investigation of Light-Weight Ceilings - Modeling aspects and Design Guidelines. Proceedings of EuroNoise 2015, Maastricht, Netherlands: 2015, p. 2497–502.

[33] Kohrmann M., Buchschmid M., Müller G., Völtl R., Schanda U. Numerical models for the prediction of vibro-acoustical characteristics of light-weighted ceilings. Proceedings of Inter-Noise 2013, Innsbruck, Austria: 2013.

[34] Olsson J., Linderholt A., Nilsson B. Impact evaluation of a thin hybrid wood based joist floor. Proceedings of ISMA2016 International Conference on Noise and Vibration Engineering and USD2016 International Conference on Uncertainty in Structural Dynamics, Leuven, Belgium: 2016, p. 589–602.

[35] Linderholt A., Olsson J. A simulation based study of low frequency transient sound radiation from floors - A concrete vs. a hybrid floor. Proceedings of International Congress on Sound and Vibration ICSV 24, London, United Kingdom: 2017, p. 23–7.

[36] Olsson J, Linderholt A. Low-frequency impact sound of timber floors: A finite element–based study of conceptual designs. Build Acoust 2021;28:17–34. https://doi.org/10.1177/1351010×20917874.

[37] Rabold A. Anwendung der Finite Element Methode auf die Trittschallberechnung. Dissertation. Technische Universität München, 2010.

[38] Rabold A., Düster A., Rank E. Anwendung der Finiten Elemente Methode auf die Trittschallberechnung von Holzdecken. Proceedings of DAGA 2007, Stuttgart, Germany: 2007, p. 261–262.

[39] Rabold A, Düster A, Rank E. FEM based prediction model for the impact sound level of floors. Proc Meet Acoust, Paris, Fr 2008:2993–8. https://doi.org/10.1121/1.2933931.

[40] Rabold A., Düster A., Hessinger J., Rank E. Optimization of lightweight floors in the low frequency range with a FEM based prediction model. Proceedings of NAG/DAGA 2009, Rotterdam, Netherlands: 2009, p. 1514–1517.

[41] Rabold A, Buchschmid M, Düster A, Müller G, Rank E. Modelling the excitation force of a standard tapping machine on lightweight floor structures. Build Acoust 2010;17:175–97. https://doi.org/10.1260/1351-010X.17.3.175.

[42] Kohrmann M. Dissertation. Technische Universität München. Numer Methods Vibro-Acoust Assess Timber Floor Constr 2017.

[43] Kohrmann M., Buchschmid M., Schanda U., Müller G. A FEM-based planning tool for the vibro-acoustic design of wooden floors at low frequencies. Proceedings of the INTER-NOISE 2016 - 45th International Congress and Exposition on Noise Control Engineering: Towards a Quieter Future, Hamburg, Germany: 2016, p. 3743–3751.

[44] Cremer L, Heckl M, Petersson BAT. Structure-Borne Sound. Berlin Heidelberg: Springer-Verlag,; 2005.

[45] Coguenanff C. Robust design of lightweight wood-based systems in linear vibroacoustics. Dissertation. Universite Paris-Est, 2016.

[46] Coguenanff C., Guigou-Carter C., Jean P., Desceliers C. Probabilistic model of the impact force spectrum for the standard ISO tapping machine. Proceedings of the 22nd International Congress on Sound and Vibration ICSV 2015, Florence, Italy: 2015, p. 5551–8.

[47] Wang P, Van hoorickx C, Lombaert G, Reynders E. Numerical prediction and experimental validation of impact sound radiation by timber joist floors. Appl Acoust 2020;162:107182. https://doi.org/10.1016/j.apacoust.2019.107182.

[48] Brunskog J, Hammer P. The interaction between the ISO tapping machine and lightweight floors. Acta Acust U Acust 2003;89:296–308.

[49] Lietzén J, Sormunen J, Pajunen S, Kylliäinen M. Simulation of impact force generated by an ISO tapping machine on a wooden slab using explicit dynamics analysis. Eng Struct 2022;270:114855. https://doi.org/10.1016/j.engstruct.2022.114855.

[50] Latvanne P. The acoustical properties and the calculation models of the wooden intermediate floor constructions (in Finnish). Master of Science Thesis. Tampere University of Technology; 2015.

[51] Amiryarahmadi N., Kropp W., Bard D., Larsson K. Time-domain model of a tapping machine. Proceedings of Forum Acusticum 2011, Aalborg, Denmark: 2011, p. 1713–8.

[52] Wittstock V. On the spectral shape of the sound generated by standard tapping machines. Acta Acust U Acust 2012;98:301–8. https://doi.org/10.3813/AAA.918513.

[53] COMSOL. Acoustics Module User's Guide. 2022.

[54] Lietzén J, Kylliäinen M, Valjakka S, Pajunen S. Vibration level reduction by floor coverings installed on wooden slabs. Build Acoust 2022;29:221–37.

[55] COMSOL. Structural Mechanics Module User's Guide. 2022.

[56] Delany ME, Bazley EN. Acoustical properties of fibrous absorbent materials. Appl Acoust 1970;3:105–16.

[57] Allard J-F, Champoux Y. New empirical equations for sound propagation in rigid frame fibrous materials. J Acoust Soc Am 1992;91:3346–53. https://doi.org/10.1121/1.402824.
[58] Oliva D, Hongisto V. Sound absorption of porous materials – Accuracy of prediction methods. Appl Acoust 2013;74:1473–9. https://doi.org/10.1016/j.apacoust.2013.06.004.
[59] Hopkins C. Sound Insulation. Oxford, United Kingdom: Elsevier Ltd,; 2007.
[60] ISO 10140–3 Acoustics – Laboratory measurement of sound insulation of building elements – Part 3: Measurement of impact sound insulation. Geneva: International Organization for Standardization; 2021.
[61] Reynders E, Wang P, Van hoorickx C, Lombaert G. Prediction and uncertainty quantification of structure-borne sound radiation into a diffuse field. J Sound Vib 2019;463:114984. https://doi.org/10.1016/j.jsv.2019.114984.
[62] Reynders E. Practical formulas for quantifying the uncertainty of impact sound insulation measurements caused by the diffuse field assumption. Proceedings of Inter-Noise 2019, Madrid, Spain: 2019.
[63] Niskanen K., Gustafsson P.-J., Berglund L., Kulachenko A., Nygards M., Hägglund R., et al. Mechanics of Paper Products. 1st ed. De Gruyter, Inc; 2011.
[64] Saint-Gobain Finland Oy (Gyproc) Gyproc Käsikirja – Kevytrakennejärjestelmät (in Finnish). Helsinki, Finland: 2022.
[65] Getzner Werkstoffe GmbH. Sylomer SR 42 Data sheet. 2019.
[66] Saint-Gobain Finland Oy (Gyproc). Tuotekortti – Gyproc GN 13 Normaali (in Finnish). 2021.
[67] Saint-Gobain Finland Oy (Gyproc). Tuotekortti – Gyproc GL 15 Lapikas – Lattialevy (in Finnish). 2021.
[68] Metsäliitto Cooperative (Metsä Wood). Kerto® LVL manual – Mechanical properties. 2021.
[69] Saint-Gobain Finland Oy (Isover). Declaration of Performance – Isover Acoustic. 2022.
[70] Saint-Gobain Finland Oy (Isover). Isover valintataulukko (in Finnish). 2022.
[71] EN 1993–1-1. Eurocode 3: Design of steel structures - Part 1–1: General rules and rules for buildings. Brussels: European Committee for Standardization; 2005.
[72] Tremco Illbruck Oy. SP925 Tekninen tiedote (in Finnish). 2022.
[73] Lietzén J, Miettinen J, Kylliäinen M, Pajunen S. Impact force excitation generated by an ISO tapping machine on wooden floors. Appl Acoust 2021;175. https://doi.org/10.1016/j.apacoust.2020.107821.
[74] LS-DYNA Keyword User's Manual, Volume I (r:8752). Livermore, California: Livermore Software Technology Corporation (LSTC); 2017.
[75] Ala-Outinen T., Hakkarainen J. Product certificate EUFI29–20000564-C - LVL G by Stora Enso. Espoo: Eurofins Expert Services Oy; 2020.
[76] ISO 717–2. Acoustics – Rating of sound insulation in buildings and of building elements – Part 2: Impact sound insulation. Geneva: International Organization for Standardization; 2020.
[77] Kylliäinen M, Lietzén J, Kovalainen V, Hongisto V. Correlation between single-number-quantities of impact sound insulation and various noise ratings of walking on concrete floors. Acta Acust U Acust 2015;101:975–85. https://doi.org/10.3813/AAA.918892.